2011

M-ary Chirp Modulation for Data Transmission

Mohammad A. Alsharef

M-ary Chirp Modulation for Data Transmission

(Spine title: M-ary Chirp Modulation for Data Transmission)

(Thesis format: Monograph)

by

Mohammad A Alsharef

Graduate Program
in
Engineering Science
Department of Electrical and Computer Engineering

2

A thesis submitted in partial fulfillment
of the requirements for the degree of
Master of Engineering Science

School of Graduate and Postdoctoral Studies
The University of Western Ontario
London, Ontario, Canada

Certificate of Examination

THE UNIVERSITY OF WESTERN ONTARIO
SCHOOL OF GRADUATE AND POSTDOCTORAL STUDIES
CERTIFICATE OF EXAMINATION

Chief Advisor:

Dr. Raveendra Rao

Advisory Committee:

Examining Board:

Dr. Abdallah Shami

Dr. Quazi Rahman

Dr. Anand Prakash

The thesis by
Mohammad A Alsharef
entitled:
M-ary Chirp Modulation for Data Transmission
is accepted in partial fulfillment of the
requirements for the degree of
Master of Engineering Science

Date: _____

Chair of Examining Board

Abstract

M-ary chirp modulations, both discontinuous- and continuous-phase, for M-ary data transmission are proposed and examined for their error rate performances in additive, white, Gaussian noise (AWGN) channel. These chirp modulated signals are described and illustrated as a function of time and modulation parameters. M-ary chirp modulation with discontinuous phase is first proposed and then the M-ary Continuous Phase Chirp Modulation (MCPCM) is considered. General descriptions of these modulation systems are given and properties of signals representing these modulations are given and illustrated. Optimum algorithms for detection of these signals in AWGN are derived and structures of optimum receivers are identified. Using the minimum Euclidean distance criterion in signal-space, upper bounds on Signal-to-Noise Ratio (SNR) gain relative to Multiple Phase Shift Keying (MPSK) are established for 2-, 4-, and 8-ary MCPCM systems. It is observed that the maximum likelihood coherent and non-coherent receivers for MCPCM are non-linear and require multiple-symbol observations. Since symbol error probability performance analyses of these receivers are too complex to perform, union upper bounds on their performances are derived and illustrated as a function of SNR, number of observation symbols, and modulation parameters for MCPCM. Optimum 2-, 4-, and 8-ary modulation schemes that minimize union upper bound on symbol error rates have been determined and illustrated. Our results show that 2-, 4-, and 8-ary optimum coherent MCPCM systems, with 5-symbol observation length, offer 1.6 dB, 3.6 dB, and 8 dB improvements relative to 2-ary, 4-ary, and 8-ary PSK systems, respectively. Also, it is shown that optimum 2-ary and 4-ary non-coherent MCPCM systems can outperform 2-ary and 4-ary coherent PSK systems, respectively.

Acknowledgements

All praise be to Allah for bestowing upon me His countless bounties.

I would like to express my sincerest gratitude to my supervisor Dr. Raveendra K. Rao who has supported me throughout my master degree study at the University of Western Ontario. Without his time, encouragement and knowledge, this thesis would not have been completed.

Acknowledgement are due to the Ministry of Higher Education, Saudi Arabia for awarding me Scholarship and for providing the necessary financial assistance throughout my study at UWO.

I would like to extend my appreciation to all my friends here at UWO with whom it has been pleasure to work with over two years. Also, I would like to thank the Electrical Engineering and Graduate Studies Department staff, including Melissa, Tracey and Charlene.

I am grateful to my parents and family for their support and encouragement over the years. The role of my parents in my upbringing and prayers have played the major role in making me what I am today.

Table of Contents

List of Tables

List of Figures

Acronyms

MCPCM	*M-ary Continuous Phase Chirp Modulation*
PAN	*Personal Area Network*
WLAN	*Wireless Local Area Network*
MAN	*Metropolitan Area Network*
TDMA	*Time Division Multiple Access*
CDMA	*Code Division Multiple Access*
OFDM	*Orthogonal Frequency Division Multiplexing*
DCS	*Digital Communication Systems*
RF	*Radio Frequency*
FDMA	*Frequency Division Multiple Access*
PSD	*Power Spectral Density*
ACI	*Adjacent Channel Interference*
BER	*Bit Error Rate*
SNR	*Signal to Noise Ratio*
EM	*Electromagnetic Interference*
FM	*Frequency Modulation*
DS	*Direct Sequence*
FH	*Frequency Hopping*
LFM	*Linear Frequency Modulation*
SAW	*Surface Acoustic Wave*
HF	*High Frequency*
DS-BPSK	*Direct-Sequence Binary Phase Shift Keying*
ISM	*Industrial Scientific and Medical*
BPSK	*Binary Phase Shift Keying*
FSK	*Frequency Shift Keying*
LPI	*Low Probability of Intercept*
MCM	*Matched Chirp Modulation*
BOK	*Binary Orthogonal Keying*

AWGN	*Additive White Gaussian Noise*
CPC	*Continuous Phase Modulation*
PAM	*Pulse Amplitude Modulation*
PAPR	*Peak-to-Average Power Ratio*
QPSK	*Quadrature Phase Shift Keying*
MSK	*Minimum Shift Keying*
MPSK	*M-ary Phase Shift Keying*
PDF	*Probability Density Function*
MFSK	*Multiple Frequency Shift Keying*
CPM	*Continuous Phase Modulation*
CPFSK	*Continuous Phase Frequency Shift Keying*

Chapter 1
Introduction

1.1 Introduction

Wireless communications has become one of the most rapidly growing industries in the world, and its products are now exerting an impact in our daily lives. Wireless communications today covers a very wide array of applications. The telecommunications industry is one of the largest industries worldwide with more than $ 1 trillion in annual revenues for service and equipment. The largest and most noticeable part of telecommunications business is telephony. The principal wireless component of telephony is mobile telephony. The worldwide growth rate in cellular telephony is very aggressive, and reports suggest that the number of cellular telephony subscriptions worldwide has now surpassed the number of wired telephony subscriptions. However, cellular telephony is only one of a very wide array of wireless technologies that are being developed very rapidly at the present time. Among other technologies are wireless Internet and other Personal Area Network (PAN) systems, Wireless Local Area Network (WLAN) systems, wireless Metropolitan Area Network (MAN) systems, and a variety of satellite systems. These technologies are supported by a number of transmission and channel assignment technologies, including Time Division Multiple Access (TDMA), Code Division Multiple Access (CDMA) and other spread-spectrum systems, Orthogonal Frequency Division Multiplexing (OFDM) and other multi-carrier systems, and high-rate single-carrier systems. All these modern technologies use the basic principles that underlie the design and analysis of Digital Communication System (DCS). In such a system, communication involves the transmission of information in digital form from source to destination. If the source output happens to be in analogue form, such as an audio or video signal, it is appropriately

converted to digital form. In any DCS, modulation plays a fundamental role and is an integral part of the system. This is especially so if it involves a radio system. In a DCS, the function of the modulator is to bridge the gap between digital data and the electrical signal required at the input to the Radio Frequency (RF) section. We may regard the modulator as a signal sub-system that maps data presented to it on to a modulated RF carrier for subsequent processing, amplification and transmission by the RF section. The modulation process determines the bandwidth occupied by the transmitted signal. Furthermore, the modulation determines the robustness of the system to channel impairments, due both to the RF sub-systems (such as phase noise and non-linearity) and the RF channel (such as multipath dispersion and fading). Thus, the appropriate choice of modulation scheme is vital for efficient operation of DCS [1],[2].

1.2 Parameters of Modulation Scheme

A radio system will be strictly limited by the regulating authorities to a certain frequency band. Often the available band will be shared among many users of the system by means of Frequency Division Multiple Access (FDMA) and, hence, the narrower the bandwidth occupied by each user, the more users can be accommodated. Bandwidth requirement is determined by the spectral occupancy of the modulated signal, usually presented as a plot of Power Spectral Density (PSD) as a function of frequency. Ideally, the PSD should be zero outside the band occupied. In practice, however, this can never be so, and the spectrum extends to infinity beyond the band. This is either because of the inherent characteristics of the modulation scheme or because of the practical implementation of filters. Thus, it is important to define the bandwidth of the modulated signal such that the signal power falling outside the band is below a specified threshold. In practice, this threshold is determined by the tolerance of the system to Adjacent Channel Interference (ACI) which is itself a feature of the modulation scheme. The bandwidth efficiency of a modulation scheme is defined by the channel data rate per unit bandwidth occupied ($r/W, bits/sec/Hz$)

The next important parameter of a modulation scheme is its Bit Error Rate (BER) performance, which is defined as the ratio of the number erroneous bits received to the total number of bits received. BER represents the probability of bit error and is often plotted as a logarithm plot against the Signal-to-Noise Ratio (SNR) in dB. The ordinate of such a graph is normally the bit-energy to noise density ratio since this results in a more system-independent measure. The noise power spectral density is usually a fundamental feature of a channel and unlike the noise power it is independent of the bandwidth of the system. Since N_0 has the dimension of $Watts/Hz$, which is same as Joule, $\frac{E_b}{N_0}$ is dimensionless. The modulator/demodulator complexity is yet another parameter that determines the choice of a modulation in any DCS. The complexity is measured in terms of the number of correlators required in the implementation of the demodulator. In a coherent demodulator, synchronization to incoming signals at the receiver is required. This will further increase the complexity of the receiver. Since coherent receiver assumes exact knowledge of the carrier waveform (phase and frequency), it is generally limited by the complexity of the required synchronization scheme. Thus, in many situations non-coherent receivers which are better suited for implementation are considered. Modulation techniques can be classified as: i) linear or non-linear and ii) memoryless or with memory. While linearity of a modulation method requires that the principle of superposition applies in the mapping of the digital sequence into successive waveforms, in a non-linear modulation, the superposition principle does not apply to signals transmitted in successive time intervals. When the mapping from a digital sequence to waveforms is performed under the constraint that a waveform transmitted in any time interval depends on one or more previously transmitted waveforms, the modulator is said to have memory. In contrast, when the mapping from the digital sequence to the waveforms is performed without any constraint on previously transmitted waveforms, the modulator is called memoryless.

The ultimate choice of a modulation scheme in a DCS depends on spectral efficiency, BER performance and receiver complexity. In general, any DCS can be viewed as a point in a three-dimensional space- power, bandwidth, and system complexity. There always exist trade-offs among these three parameters in the design of a DCS.

In practice, we find two types of modulations: one optimized for power and the other optimized for bandwidth. The choice of which one is preferred depends on whether the DCS in question is power-limited or bandwidth-limited. Accordingly, we refer to modulation schemes as either power-efficient or bandwidth-efficient.

1.3 Chirp Spread Spectrum Systems

While the prime issue of concern in the study of DCS is that of providing for efficient use of power and bandwidth, there exist situations where one sacrifices these efficiencies in order to meet other design objectives such as to provide secure communication in a hostile environment. A major advantage of such a system is its ability to reject interference, be it intentional or unintentional. The class of signals that cater to this requirement is referred to as spread-spectrum modulation. In recent years, indoor wireless communication has gained increasing attention and its market share is expected to grow rapidly in the coming years due to its advantages over cable networks such as mobility of users, elimination of cabling and flexibility etc. Typical applications are cordless phone systems, WLANs for home and office applications and flexible mobile data transmission links between sensors, actuators, robots, and controller units in industrial environments. Due to the hostile electromagnetic (EM) environment, which includes severe EM emissions from other devices as well as distortions due to multipath propagation, the robustness of the communication link is an extremely important feature in a wireless communication system. The spread-spectrum technology is well suited to provide robust data transmission in these applications.

In a spread-spectrum system, the transmitted signal is spread over a wide frequency band, often much wider than the minimum bandwidth required for conveying the information. An instance of spectrum spreading may be seen in conventional Frequency Modulation (FM), by employing frequency deviations greater than unity. The wideband FM thus produced is often classified as a spread-spectrum system because the RF spectrum produced is much wider than that of the transmitted information. While in FM, the transmitted bandwidth is a function of both information

bandwidth and the amount of modulation, there are techniques in which spectrum spreading is accomplished using some signal or operation other than the information bearing signal that is transmitted. For example, in Direct Sequence (DS) and Frequency Hopping (FH) spread spectrum systems, the spreading and despreading functions are used in the transmitter and receiver, respectively [2]. In these spread spectrum systems, the synchronization of the despreading code is difficult and needs high computational effort. Linear Frequency Modulation (LFM) or chirp modulation is another type of spread spectrum signalling technique in which a carrier is swept over a wideband during a given data pulse interval. Chirp modulation [3],[4] does not necessarily employ coding and produces a transmitted bandwidth much greater than the bandwidth of the information being transmitted. The growing interest in chirp modulation is mainly due to the advances in Surface Acoustic Wave (SAW) technology, which offers a rapid close-to-optimum method for both generation and correlation of wideband chirp pulses [5]. Chirp systems have found major applications in radar systems for reasons such as anti-eavesdropping, anti-interference and low-Doppler sensitivity. Among several applications of chirp signals in communication are radio telephony, cordless systems, air-ground communication via satellite repeaters, data communication in the High Frequency (HF) band and WLANs. In 2007, IEEE introduced Chirp Spread Spectrum (CSS) physical layer in the new wireless standard 802.15.4a [6]. Additionally, this standard uses chirp modulation with no additional coding, whereas in 802.15.4 standard, direct-sequence binary phase shift keying (DS-BPSK) and additional spreading codes are used. This new standard targets applications such as industrial and safety control, sensor actuator networking, and medical and private communication devices. By applying CSS techniques to multidimensional multiple-access modulation, single-chirp transceivers for wireless communication in the industrial, scientific, and medical (ISM) band have been developed and are commercially available [7].

1.4 Literature survey, motivation, and objectives

The linear FM or chirp modulation technique has been extensively used in radar systems to solve the conflicting requirements of simultaneous long range and high resolution performance [8]. Winkler [9], who was motivated by the anti-interference, anti-eavesdropping, and low-Doppler sensitivity properties of chirp signals, considered chirp modulation for binary data transmission. In her work, she used two chirp signals, up-chirp (sinusoidal signal whose frequency increases linearly with time) and down-chirp (sinusoidal signal whose frequency decreases linearly with time), to map binary data for transmission of digital teletype, voice and telemetry signals. Berni and Gregg [10] investigated the performance of chirp modulation in terms of its probability of bit error rate and spectrum usage and compared them with the performances of BPSK and binary FSK techniques. They concluded that BPSK is superior in performance compared to binary FSK and binary chirp modulation. Gott and Newsome [11] proposed wideband chirp signals for data transmission in the HF band and evaluated the performance of these signals experimentally. They concluded that by using orthogonal signals and matched filter detection, both narrowband and wideband systems offer equivalent performance for the same bit energy. In [12], Dayton extended the concept of chirp modulation for data transmission using satellites in the HF band. Gott and Karia [13] subsequently applied the concept of differential encoding technique for binary data transmission using chirp signals. In [14], Kowatsch et. al. investigated the anti-jam performance of a combined PSK and chirp signal system. They have concluded that such a system can assure Low Probability of Intercept (LPI) and hence better anti-jam performance. In [15], Elkhamy and Shaaban introduced a new class of chirp modulation referred to as Matched Chirp Modulation (MCM), which is an improved version of the conventional chirp modulation. They have analysed the performance of MCM using optimum non-coherent and partially coherent receivers. It is shown that MCM offers good performance over dispersive communication channels. Combining the chirp signalling technique with some kind of pseudo-random coding, it is possible to achieve a substantial improvement in anti-jam performance. Such a system is presented and analysed in [16] by Elhakeem and

Targi. In [17], Kowatsch and Lafferl presented a spread spectrum transmission system that uses a combination of chirp modulation and pseudo-random PSK. In [18]. Wang, Fei, and Li have proposed a structure for the chirp Binary Orthogonal Keying (BOK) system and have obtained an expression for the probability of bit error. It is shown that chirp BOK performs better than traditional BOK modulation in Additive White Gaussian Noise (AWGN) channel. In all the above chirp systems, binary data transmission and receivers that are required to make independent bit-by-bit decisions are considered. In [19], Hirt and Pasupathy considered binary chirp signals by introducing phase continuity at bit transitions. They demonstrated that coherent binary phase continuous chirp (CPC) modulation can offer, at most, 1.66 dB improvement over BPSK. They have extended this work to non-coherent situation in [20]. In [21], Raveendra considered binary phase continuous chirp modulation with time-varying modulation parameters referred to as dual-mode binary chirp modulation and has shown that it can outperform binary CPC modulation. More recently, in [22] , Bhumi and Raveendra have considered digital asymmetric phase continuous chirp signals for data transmission and have shown that it can outperform dual-mode chirp modulation considered in [21] . In recent years, there have been a number of publications [21], [23, 24, 25, 26, 27, 28] that clearly exhibit the choice of chirp modulation in a variety of digital communication systems. It is well known that M-ary signalling schemes can be used for reducing the bandwidth requirements of baseband Pulse Amplitude Modulation (PAM) data transmission systems [2]. M-ary digital modulation schemes are preferred over binary digital modulation schemes for transmitting digital information over bandpass channels when one wishes to conserve bandwidth (at the expense of increasing power requirements), or to conserve power (at the expense of increasing bandwidth requirements). In practice, we seldom find a channel that has the exact bandwidth required for transmitting the output of source using binary signalling schemes. M-ary schemes may be used to utilize the additional bandwidth to provide increased immunity to channel noise. Thus, in this thesis, we examine the more general case of M-ary data transmission using chirp modulation. Firstly, we consider memoryless chirp modulation for M-ary data transmission. Both coherent and non-coherent detection situations in AWGN channel are considered. Structures

of optimum coherent and non-coherent receivers are derived and closed-form expressions for their BER performances are obtained. The optimum M-ary chirp systems have been determined through minimization of bit error rates. Next, we consider the case of M-ary data transmission using chirp modulation with memory. The class of signals will be referred to as M-ary Continuous Phase Chirp Modulation (MCPCM). The ability of these signals to operate over AWGN channel is estimated using the criteria of minimum Euclidean distance. The problem of coherent and non-coherent detection of MCPCM signals in AWGN channel is then addressed and structures of optimum receivers are derived using composite hypothesis detection theory. The error rate upper bounds on these receivers are then derived using the union bound. Using numerical minimization of error rate bound, optimum 2-, 4, and 8-ary MCPCM systems have been determined. Finally, A comparison of the performance of M-ary chirp modulation relative to other conventional M-ary modulations is also provided.

1.5 Thesis organization

In Chapter 2, the signals that describe M-ary chirp modulation are described and illustrated. Firstly, memoryless M-ary chirp modulation is described and signals that describe the modulation are given and illustrated. Secondly, M-ary chirp modulation with memory, referred to as MCPCM, are described and illustrated. The parameters that affect the modulation process are described and illustrated. Finally, some properties of chirp modulated signals are sketched.

The problem of detection of memoryless M-ary Chirp modulated signals in additive, white, Gaussian noise is addressed in Chapter 3 and the structures of optimum coherent and non-coherent receivers are derived. Closed-form expressions for symbol error rates of these optimum receivers are derived and illustrated as a function of modulation parameters. A comparison of error rate performance of M-ary chirp modulations with other conventional M-ary modulations is also provided.

In Chapter 4, we examine the continuous phase chirp signals for M-ary data transmission. Using the notion of minimum Euclidean distance in signal-space, the achievable SNR gains relative to PSK systems are established. The optimum and

sub-optimum receiver structures for coherent detection, and arbitrary number of observation intervals, are derived and their performances in terms of symbol error rates are given. It is shown that the symbol error rate upper bound on the performance of the optimum coherent receiver is a function of the signal modulation parameters, the receiver decision observation length, number of levels of data, and the received signal-to-noise ratio. It is shown that 2-ary MCPCM system over $5T$ observation offers nearly 1.6 dB improvement relative to coherent PSK, 4-ary MCPCM system has nearly 3.6 dB gain over QPSK, and 8-ary MCPCM system over $5T$ observation length offers approximately 8 dB improvement relative to 8-ary PSK system.

In Chapter 5, optimum non-coherent MCPCM receiver is derived and the symbol error rate of this receiver is determined using the high-SNR union upper bound. Explicit expressions for determining this upper bound have been obtained. Parameters that influence the performance of the optimum non-coherent receiver have been identified. It is shown that 2-ary and 4-ary non-coherent MCPCM systems can outperform coherent PSK and coherent QPSK. Also, it is shown that non-coherent octal MCPCM modulation has up to 1.3 dB gain over coherent octal PSK.

In Chapter 6, the contributions of this thesis and the conclusions from the results obtained are summarized. Also, we outline areas for further research in the light of the needs of modern reliable communication systems.

Chapter 2
M-ary Chirp Signalling Technique

2.1 Introduction

In this Chapter, we describe two types of M-ary chirp modulations. i) M-ary chirp modulation without memory, and ii) M-ary chirp modulation with memory. While the former technique is commonly referred to as M-ary chirp modulation with discontinuous phase the latter is referred to as M-ary continuous phase chirp modulation (MCPCM). The chirp modulated signal is sketched as a function of time and the modulation parameters are illustrated . Finally, the phase property of MCPCM signals are illustrated.

2.2 M-ary Data Transmission System

The partial block diagram, that consists of information source and digital modulators, of a typical digital communication system is shown in Fig. 2.1. Blocks such as source encoder and channel encoder are omitted and are not part of the research presented in this thesis. The source output may be either an analog signal, such as an audio or video signal, or digital signal such as the output of a computer. In a DCS, the message produced by the source are assumed to be sequence of binary digits. This binary sequence is passed to an accumulator which accumulates K binary digits (and assigns unique amplitude level) before presenting it to the digital modulator. When $K = 1$, the digital modulator simply maps binary digits 0 to a waveform $S_1(t)$ and the binary digit 1 to a waveform $S_2(t)$, both over the bit interval of T_b sec. We call this binary modulation. Alternatively, the modulator may transmit K information bits at a time by using $M = 2^k$ distinct waveforms $S_i(t), i = 1, 2, \ldots, M$, one waveform for

each of the 2^k possible $K-bit$ sequence. We call this M-ary modulation ($M > 2$). If R is the bit rate of the input source, then a new $K-bit$ sequence enters the modulator every K/R seconds. Thus, when the channel bit rate R is fixed, the amount of time available to transmit one of the M waveforms corresponding to a $K-bit$ sequence is K times the time period in a system that uses binary modulation.

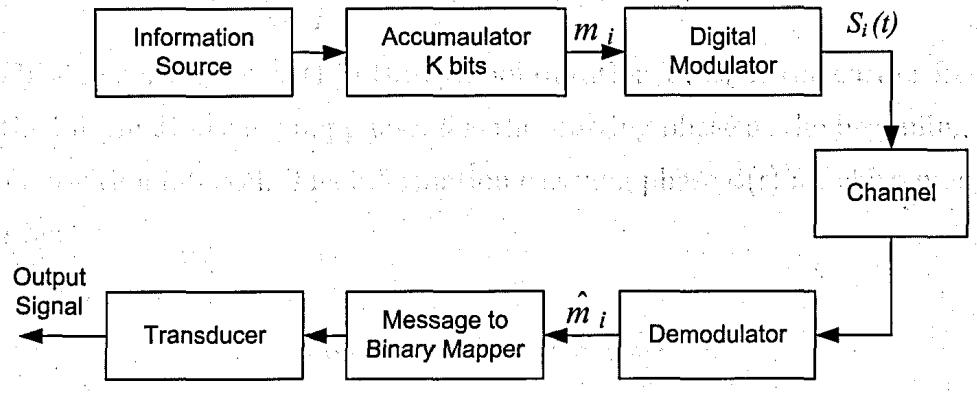

Figure 2.1: Partial Block Diagram of DCS

The communication channel is the medium that is used to send the signal from the transmitter to the receiver. Whatever the physical medium used for transmission of information, the essential feature is that the transmitted signal is corrupted in random manners by a variety of possible mechanisms. The simplest mathematical model for a communication channel is the additive noise channel. In this thesis, we model the additive noise channel to be white and Gaussian, with one-sided power spectral density of N_0 $watts/Hz$. Because this channel model applies to a broad class of physical communication channel and because of its mathematical tractability, this is the predominant channel model used in our communication system design and analysis.

At the receiver end of a digital communication system, the digital demodulator processes the channel-corrupted transmitted waveform and reduces the waveforms to a sequence of numbers that represent the estimates of the data symbols which is

subsequently converted into a sequence of binary digits that represent the estimate of the source output at the transmitter.

2.3 Memoryless M-ary Chirp Modulation

The general expression for M-ary chirp modulated signal is given by:

$$S(t) = \sqrt{\frac{2E_s}{T}} \cos(w_c t + \phi(t) + \theta), \quad 0 \leq t \leq T \tag{2.1}$$

where E_s is the energy of $S(t)$ in the symbol duration T, w_c is the carrier frequency, $\phi(t)$ is the information carrying phase, θ is the starting phase at the beginning ($t = 0$) of the observation interval. The information carrying phase $\phi(t)$ for chirp modulation is given by:

$$\phi(t) = a_1 g(t), \quad 0 \leq t \leq T \tag{2.2}$$

where a_1 is the M-ary data taking one of the values $\pm 1, \pm 3, \ldots, \pm(M-1)$ The phase function $g(t)$ is given by:

$$g(t) = \begin{cases} 0, & t \leq 0, \ t>T \\ 2\pi \int_0^t f_d(\tau) d\tau, & 0 \leq t \leq T \\ \pi q, & t = T \end{cases} \tag{2.3}$$

and $f_d(t)$ is the instantaneous frequency deviation. For chirp signalling

$$f_d(t) = \begin{cases} 0, & t \leq 0, \ t>T \\ \frac{h}{2T} - \frac{w}{T^2} t, & 0 \leq t \leq T \end{cases} \tag{2.4}$$

Using (2.4) in (2.3), (2.2) can be written as

$$\phi(t) = \begin{cases} 0, & t \leq 0, \ t>T \\ \pi a_1 \left\{ h\left(\frac{t}{T}\right) - w\left(\frac{t}{T}\right)^2 \right\}, & 0 \leq t \leq T \\ \pi a_1 q = \pi a_1 (h - w), & t = T \end{cases} \tag{2.5}$$

where h and w are dimensionless parameters: h represents the initial peak-to-peak frequency deviation divided by the bit rate $1/T$, and w represents the frequency sweep width divided by the bit rate $1/T$. Since $h = (q + w)$, we may choose (w, q) to be independent signal modulation parameters.

2.3.1 Binary Chirp Modulation

In binary chirp modulation, data a_1 takes values ± 1. Fig. 2.2 shows the block diagram of chirp modulator for binary data. In binary chirp modulation, the modulator outputs up-chirp signal, $S_1(t)$, or down-chirp signal, $S_2(t)$ accordingly as the input is a binary '1' or '0', respectively. This is summarized below for the case of $\theta = 0$:

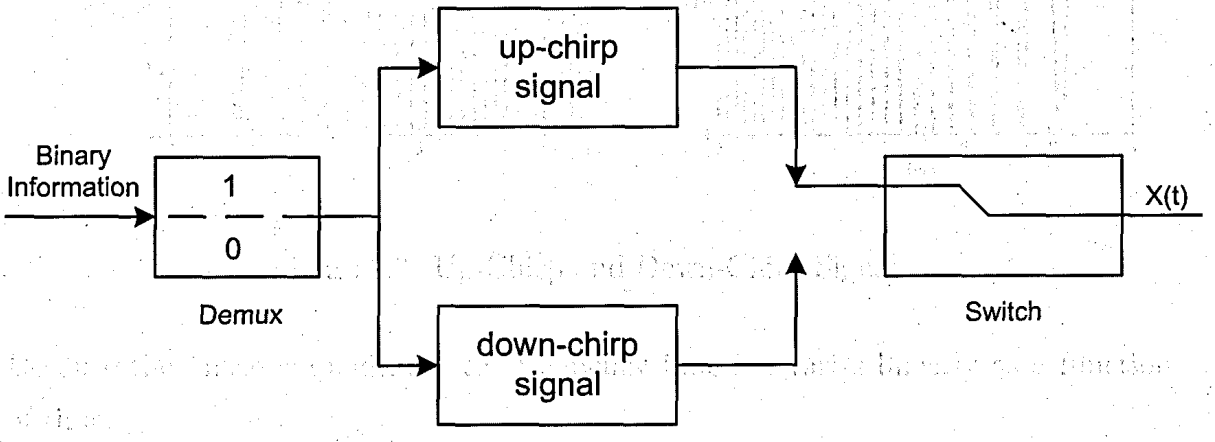

Figure 2.2: Block Diagram of Binary chirp Modulation

$$\text{'1'} \longrightarrow +1 \longrightarrow S_1(t) = \sqrt{\frac{2E_b}{T_b}} \cos\left[w_c t + \pi\left\{h\left(\frac{t}{T_b}\right) - w\left(\frac{t}{T_b}\right)^2\right\}\right], \quad 0 \le t \le T_b$$

$$\text{'0'} \longrightarrow -1 \longrightarrow S_2(t) = \sqrt{\frac{2E_b}{T_b}} \cos\left[w_c t - \pi\left\{h\left(\frac{t}{T_b}\right) - w\left(\frac{t}{T_b}\right)^2\right\}\right], \quad 0 \le t \le T_b \tag{2.6}$$

Fig. 2.3 shows waveforms in (2.6) as a function of time. In Fig. 2.4, the phase and frequency functions are shown for binary chirp signals for $q > 0, q = 0$, and $q < 0$.

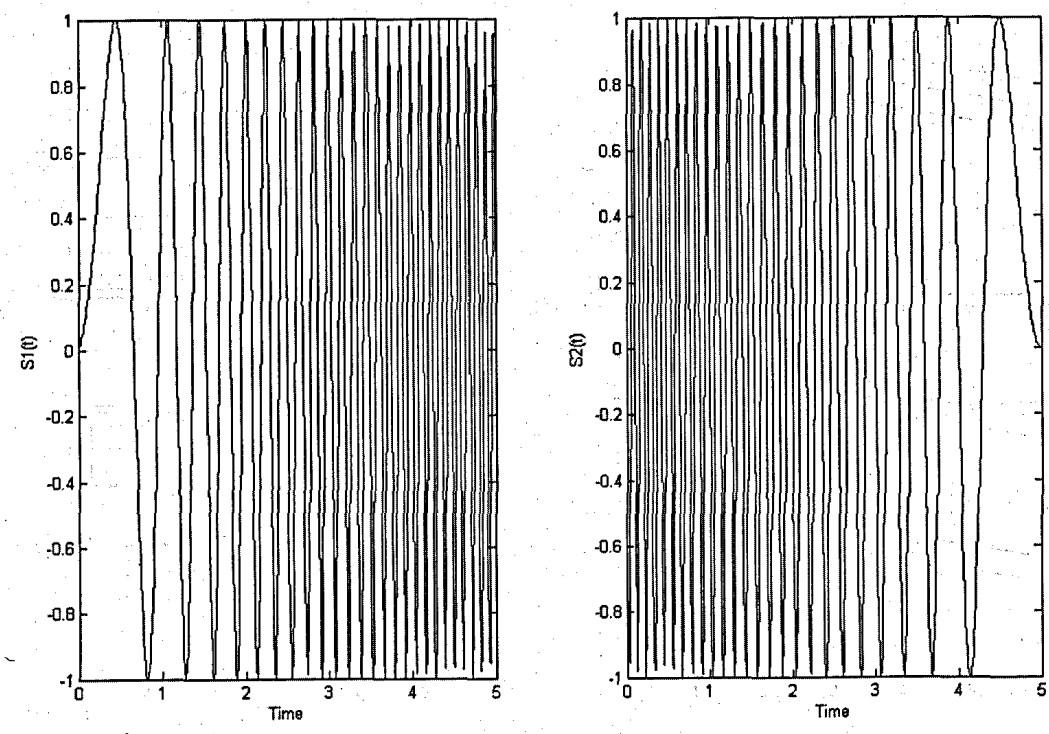

Figure 2.3: Up-Chirp and Down-Chirp Signals

Because the phase is quadratic, the frequency function varies linearly as a function of time.

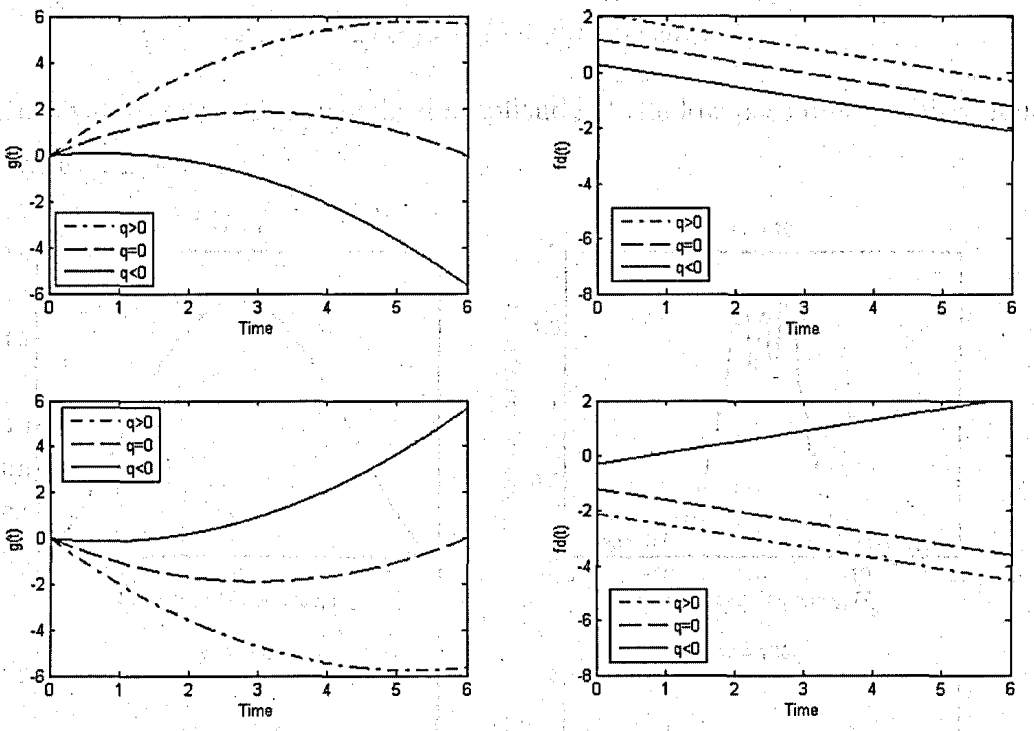

Figure 2.4: Instantaneous Phase and Frequency of Binary Chirp Signal

- Spectrum of Binary Chirp Signals

The binary chirp signal spectrum can can be found by:

$$\mathfrak{G}(f) = \int_0^T \cos(2\pi f_c t + d_i \pi \left\{ h\left(\frac{t}{T_b}\right) - w\left(\frac{t}{T_b}\right)^2 \right\} e^{-j2\pi f_c t} dt \qquad (2.7)$$

and after solving the integral in (2.7) , the spectrum is given by:

$$\mathfrak{G}(f) = exp(-j\phi)\left\{[C(x_+) - C(x_-)] + j[S(x_+) - S(x_-)]\right\} \qquad (2.8)$$

where

$$\phi = \pi[T_s(f_c - f) + d_i h/2]^2/d_i w$$

$$x_+ = [2d_i - d_i h - 2T_s(f_c - f)]/\sqrt{2d_i w}$$

and

$$x_{-} = -[2T_s(f_c - f) + d_i h]/\sqrt{2d_i w}$$

For different values of w,the normalized amplitude of the low pass binary chirp signal is shown in Fig. 2.5

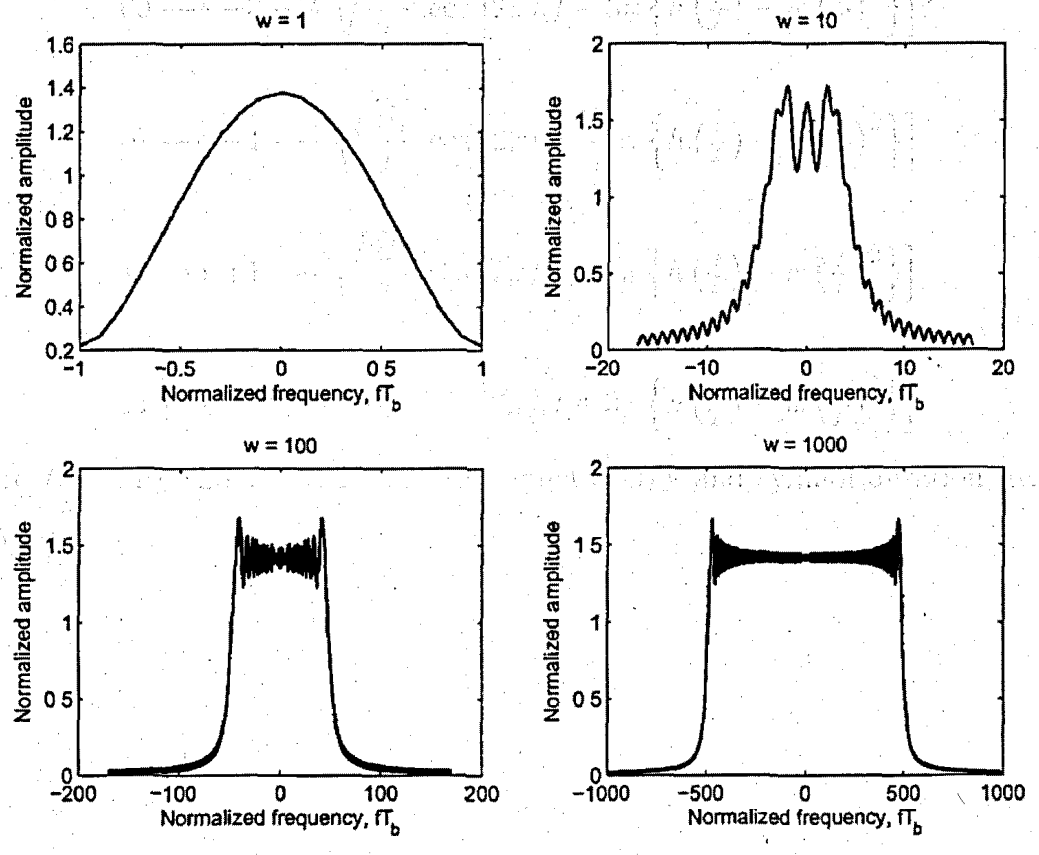

Figure 2.5: Spectrum of Binary Chirp Signal [29]

2.3.2 4-ary Chirp Modulation

In 4-ary chirp modulation, the data a_1 takes values $\pm 1, \pm 3$. Using (2.1), the four possible modulated signals can be written as:

$$\begin{aligned}
00 \longrightarrow -3 &\longrightarrow \sqrt{\frac{2E}{T}} \cos\left[2\pi f_c t - 3\pi\left\{h\left(\tfrac{t}{T}\right) - w\left(\tfrac{t}{T}\right)^2\right\}\right] \\
01 \longrightarrow -1 &\longrightarrow \sqrt{\frac{2E}{T}} \cos\left[2\pi f_c t - 1\pi\left\{h\left(\tfrac{t}{T}\right) - w\left(\tfrac{t}{T}\right)^2\right\}\right] \\
10 \longrightarrow +1 &\longrightarrow \sqrt{\frac{2E}{T}} \cos\left[2\pi f_c t + 1\pi\left\{h\left(\tfrac{t}{T}\right) - w\left(\tfrac{t}{T}\right)^2\right\}\right] \\
11 \longrightarrow +3 &\longrightarrow \sqrt{\frac{2E}{T}} \cos\left[2\pi f_c t + 3\pi\left\{h\left(\tfrac{t}{T}\right) - w\left(\tfrac{t}{T}\right)^2\right\}\right]
\end{aligned} \tag{2.9}$$

Where $E = 2E_b$ and $T = 2T_b$ denote symbol energy and symbol duration, respectively.

2.3.3 8-ary Chirp Modulation

In 8-ary chirp modulation, the data symbol a_1 takes values $\pm1, \pm3, \pm5, \pm7$. Hence there are 8 possible modulator outputs. They are:

$$
\begin{aligned}
000 &\longrightarrow -7 \longrightarrow \sqrt{\frac{2E}{T}}\ \cos\left[2\pi f_c t - 7\pi\left\{h\left(\tfrac{t}{T}\right) - w\left(\tfrac{t}{T}\right)^2\right\}\right] \\
001 &\longrightarrow -5 \longrightarrow \sqrt{\frac{2E}{T}}\ \cos\left[2\pi f_c t - 5\pi\left\{h\left(\tfrac{t}{T}\right) - w\left(\tfrac{t}{T}\right)^2\right\}\right] \\
010 &\longrightarrow -3 \longrightarrow \sqrt{\frac{2E}{T}}\ \cos\left[2\pi f_c t - 3\pi\left\{h\left(\tfrac{t}{T}\right) - w\left(\tfrac{t}{T}\right)^2\right\}\right] \\
011 &\longrightarrow -1 \longrightarrow \sqrt{\frac{2E}{T}}\ \cos\left[2\pi f_c t - 1\pi\left\{h\left(\tfrac{t}{T}\right) - w\left(\tfrac{t}{T}\right)^2\right\}\right] \\
100 &\longrightarrow +1 \longrightarrow \sqrt{\frac{2E}{T}}\ \cos\left[2\pi f_c t + 1\pi\left\{h\left(\tfrac{t}{T}\right) - w\left(\tfrac{t}{T}\right)^2\right\}\right] \\
101 &\longrightarrow +3 \longrightarrow \sqrt{\frac{2E}{T}}\ \cos\left[2\pi f_c t + 3\pi\left\{h\left(\tfrac{t}{T}\right) - w\left(\tfrac{t}{T}\right)^2\right\}\right] \\
110 &\longrightarrow +5 \longrightarrow \sqrt{\frac{2E}{T}}\ \cos\left[2\pi f_c t + 5\pi\left\{h\left(\tfrac{t}{T}\right) - w\left(\tfrac{t}{T}\right)^2\right\}\right] \\
111 &\longrightarrow +7 \longrightarrow \sqrt{\frac{2E}{T}}\ \cos\left[2\pi f_c t + 7\pi\left\{h\left(\tfrac{t}{T}\right) - w\left(\tfrac{t}{T}\right)^2\right\}\right]
\end{aligned}
\tag{2.10}
$$

2.4 M-ary Chirp Modulation with Memory

This class of signals will be referred to as M-ary Continuous Phase Chirp Modulation (MCPCM). The MCPCM waveform during the first symbol interval can be expressed as:

$$S(t) = \sqrt{2S}\ \cos(2\pi f_c t + a_1 g(t) + \theta), \quad 0 \leq t \leq T \tag{2.11}$$

where $g(t)$ is the phase function as given in (2.3), a_1 is the M-ary data symbol (taking one of the values $\pm 1, \pm 3, \pm 5, \ldots, \pm(M-1)$), θ is the phase of the RF carrier at the beginning of the observation interval, h and w are the modulation parameters ($q = h - w$). The accumulated phase at the end of the first symbol interval is given by $a_1 \pi q = a_1 \pi (h - w)$. In MCPCM, this ending phase during the first symbol interval will be constrained equal to the starting phase during the second symbol interval. Thus, the signal during second symbol interval can be written as:

$$S(t) = \sqrt{2S}\ \cos(2\pi f_c t + a_2 g(t - T) + a_1 \pi q + \theta), \quad T \leq t \leq 2T \tag{2.12}$$

where a_2 is the data symbol during the second symbol interval. Using the same logic, the waveform during the ith symbol interval can be written as:

$$S(t) = \sqrt{2S}\ \cos\left(2\pi f_c t + a_1 g(t - (i-1)T) + \pi q \sum_{j=1}^{i-1} a_j + \theta\right), \quad (i-1)T \leq t \leq iT \tag{2.13}$$

It is noted that the MCPCM signal during the ith symbol interval is not only a function of the data during that symbol interval, a_i, but also is a function of the past data symbols,$a_1, a_2, \ldots, a_{i-1}$, that entered the modulator. Thus, by constructing the phase to be continuous at symbol transitions, we introduce memory into the MCPCM signal. This memory can be exploited to reduce the symbol error rate at the receiver by observing the received waveform over more than one symbol interval. As described

above, MCPCM is a non-linear modulation technique with memory. The information carrying phase in (2.13) can be written as (assuming $\theta = 0$):

$$\phi(t, \tilde{a}) = a_i \pi \left\{ h\left(\frac{t}{T}\right) - w\left(\frac{t}{T}\right)^2 \right\} + \pi q \sum_{j=1}^{i-1} a_j, \quad (i-1)T \leq t \leq iT \tag{2.14}$$

It is instructive to sketch the set of phase trajectories generated by (2.14) by all possible values of the transmission sequence $\tilde{a} = a_1, a_2, \ldots, a_n$. For example, in the case of 2-ary (binary) MCPCM with binary symbols $a_i = \pm 1, i = 1, 2$, the set of trajectories beginning at time $t = 0$ is shown in Fig. 2.6 for arbitrary set of modulation parameters (w, q). For comparison, the phase trajectories for 4-ary (quaternary) is shown in Figs. 2.7. These phase diagrams are called phase trees. It is noted that the phase tree for MCPCM are piecewise continuous and do not contain discontinuities.

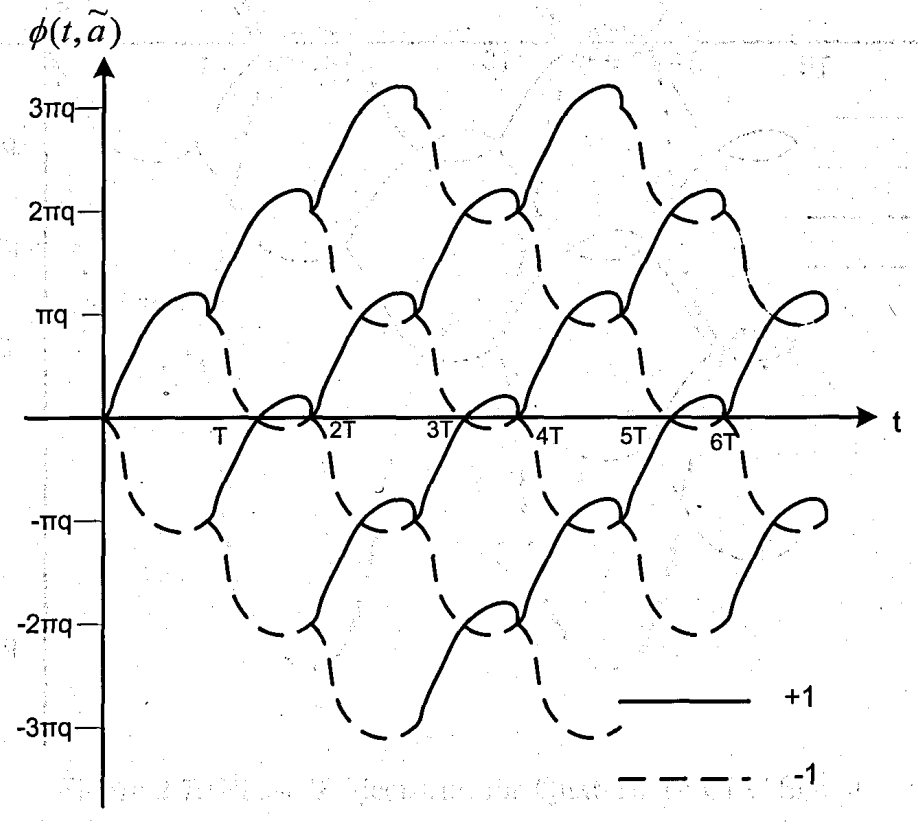

Figure 2.6: Phase Trajectories for Binary CPC Signal

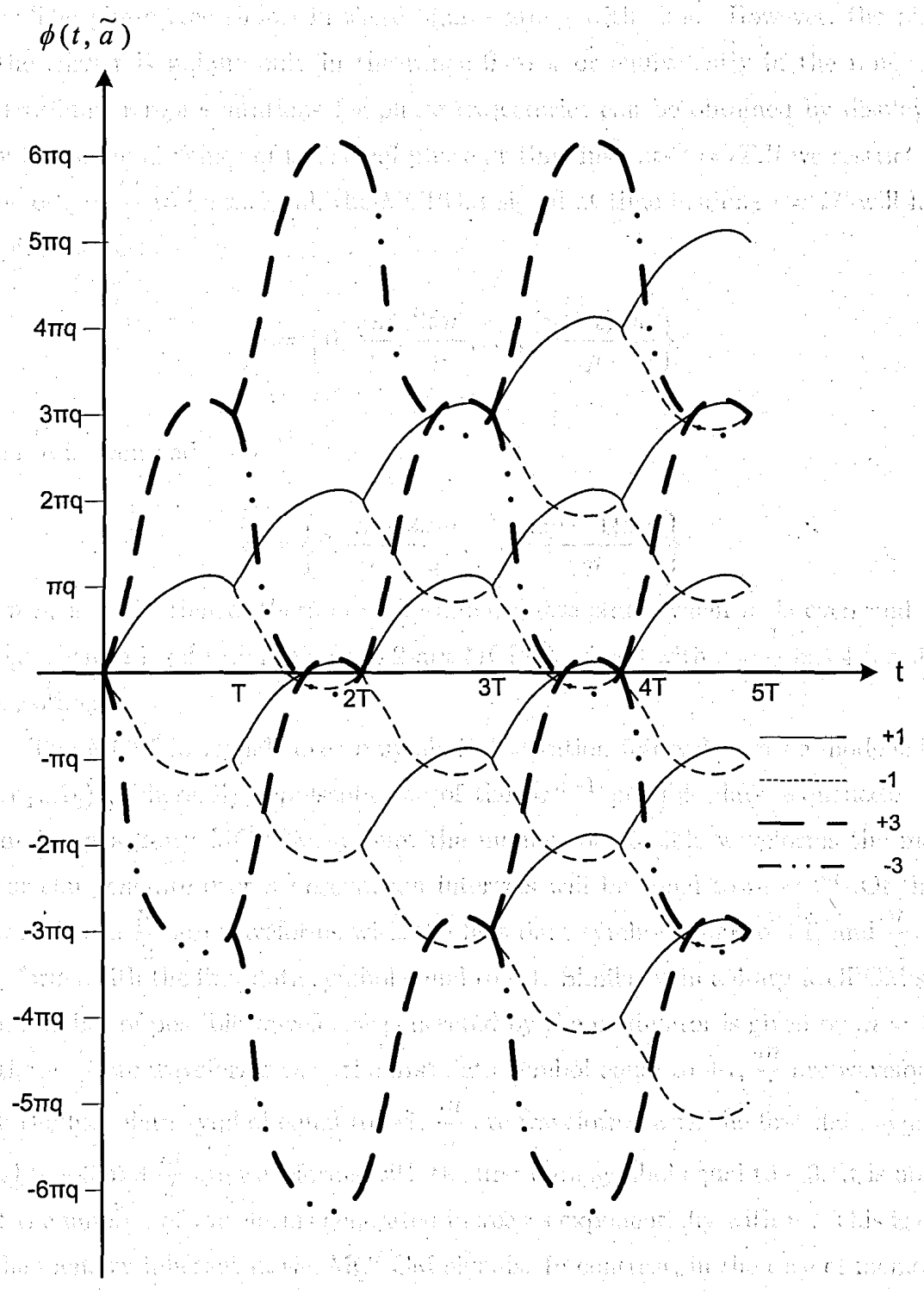

Figure 2.7: Phase Trajectories for Quaternary CPC Signal

The phase tree shown in these figures grows with time. However, the phase of the carrier is unique only in the range 0 to π or equivalently in the range $-\pi$ to $+\pi$.Simpler representations for phase trajectories can be obtained by displaying only the nominal values of the signal phase at time instants $t = iT$.If we restrict the value of $q = \frac{m}{p}$ to be rational, the MCPCM signal at time instants $t = iT$ will have terminal states:

$$\Theta = \left\{0, \frac{\pi m}{p}, \frac{2\pi m}{p}, \ldots, \frac{(p-1)\pi m}{p}\right\}$$

when m is even and

$$\Theta = \left\{0, \frac{\pi m}{p}, \frac{2\pi m}{p}, \ldots, \frac{(2p-1)\pi m}{p}\right\}$$

when m is odd. Hence, there are p terminal phase states when m is even and 2 p states when m is odd. For example, 2-ary MCPCM signal with $q = \frac{1}{2}$ has 4 terminal phase states.

The MCPCM signals over n symbol observation intervals can be modelled as $S(t, a_1, A_k)$, where A_k represents one of the M^{n-1} possible data sequences. For example, in a 2-ary MCPCM system, the number of possible waveforms the modulator can generate over n observation intervals will be equal to $m = 2^n$ .Of these m waveforms, $\frac{m}{2}$ are waveforms with the first data symbol equal to $+1$, and $\frac{m}{2}$ are waveforms with the first data symbol equal to -1. Similarly, in a 4-ary MCPCM system, number of possible waveforms generated by the modulator is given by $m = 4^n$. Of these,$\frac{m}{4}$ are waveforms with the first data symbol equal to $+1$, $\frac{m}{4}$ are waveforms with the first data symbol equal to -1, $\frac{m}{4}$ are waveforms with the first data symbol equal to $+3$ and $\frac{m}{4}$ are waveforms with the first data symbol equal to -3. It is noted that the number of waveforms generated increases exponentially with n . This is due to the memory inherent in the MCPCM signals. In contrast, in the case of memoryless M-ary chirp modulation, the number of possible waveforms in any observation interval remains equal to the value of M .

2.5 Summary

In this Chapter, we have described the signalling technique for two types of M-ary chirp modulations. Firstly, M-ary chirp modulation without memory has been explained with modulation parameters that affect the modulation process. Three different examples of M-ary chirp modulation are provided with their signals. Secondly, M-ary continuous phase chirp modulation (MCPCM) which is also referred to as M-ary chirp modulation with memory is described. Phase trees for binary and quaternary continuous chirp signals are sketched and the phase continuity property is illustrated in these examples.

Chapter 3
Detection and Performance of M-ary Chirp Modulation

3.1 Introduction

In this Chapter, the problem of coherent and non-coherent detection of M-ary chirp signals in AWGN is addressed. Structures of optimum receiver are derived and closed-form expression for their symbol error rate performance are given. Optimum M-ary chirp system have been arrived at by minimizing these symbol error rate. A comparison of the performance of these optimum M-ary chirp systems relative to conventional M-ary systems such as MFSK and MPSK is also provided.

3.2 Coherent Detection of M-ary Chirp Signals

The detection problem can be stated as an M-ary Hypothesis testing problem given by:

$$\left.\begin{array}{l} H_1 : r(t) = S_1(t) + n(t) \\ H_2 : r(t) = S_2(t) + n(t) \\ \quad\vdots \\ H_M : r(t) = S_M(t) + n(t) \end{array}\right\} \quad 0 \le t \le T \tag{3.1}$$

where $S_1(t) \ldots S_M(t)$ are the M chirp modulated signals and $n(t)$ is the additive white Gaussian noise with one-sided spectral density of N_0 $watts/Hz$. The detection problem is to observe the $S_i(t)$ in noise and to produce an optimum decision as to which of the M chirp signals, $\{S_i(t), i = 1, 2, \ldots, M\}$, was transmitted. The solution

to this problem is the likelihood ratio test and for M-ary chirp signals, the test will determine M likelihood functions given by:

$$\begin{aligned} \rho_1 &= \exp\left(\frac{2}{N_0}\int_0^T r(t)S_1(t)dt\right) \\ \rho_2 &= \exp\left(\frac{2}{N_0}\int_0^T r(t)S_2(t)dt\right) \\ &\vdots \\ \rho_M &= \exp\left(\frac{2}{N_0}\int_0^T r(t)S_M(t)dt\right) \end{aligned} \tag{3.2}$$

Taking logarithms on both sides and then multiplying both sides by $\frac{N_0}{2}$, we obtain:

$$\begin{aligned} \Lambda_1 &= \int_0^T r(t)S_1(t)dt \\ \Lambda_2 &= \int_0^T r(t)S_2(t)dt \\ &\vdots \\ \Lambda_M &= \int_0^T r(t)S_M(t)dt \end{aligned} \tag{3.3}$$

The optimum receiver will compute the M log likelihood functions $\Lambda_1, \Lambda_2, \ldots, \Lambda_M$ and arrive at the optimum decision based on the largest of these M values. Thus, the decision rule is:

$$\Lambda_k = \max\{\Lambda_1, \Lambda_2, \ldots, \Lambda_M\} \tag{3.4}$$

The M chirp modulated signals can be written as:

$$S_i(t) = \begin{cases} \sqrt{\frac{2E}{T}}\cos\left(w_c t + i\pi\left\{h\left(\frac{t}{T}\right) - w\left(\frac{t}{T}\right)^2\right\}\right), & i \ \ odd \\ \sqrt{\frac{2E}{T}}\cos\left(w_c t - (i-1)\pi\left\{h\left(\frac{t}{T}\right) - w\left(\frac{t}{T}\right)^2\right\}\right), & i \ \ even \end{cases} \tag{3.5}$$

where i takes values $1, 2, \ldots, M$. Thus, the decision rule of (3.4) will produce the output to be either k or $-(k-1)$ to be the most likely symbol transmitted, accordingly as k is odd or even. For example, if $k = 5$, the receiver decides symbol $+5$ was transmitted. On the other hand, if $k = 4$, the receiver would decide $-(k-1) = -3$ was transmitted. The structure of the receiver dictated by (3.4) is shown in Fig. 3.1.

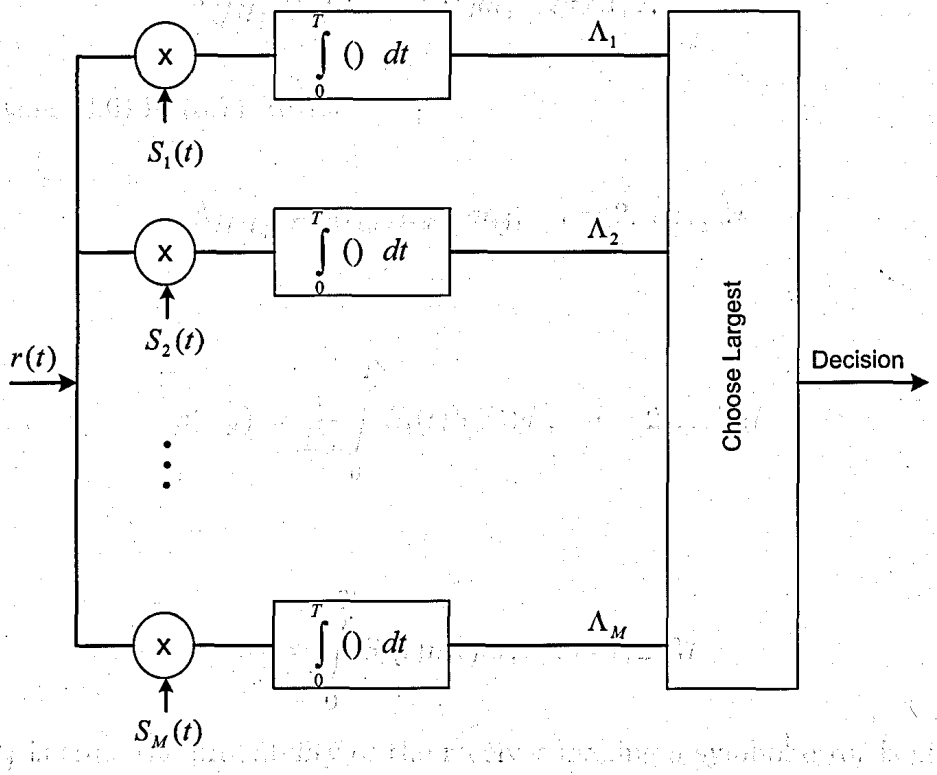

Figure 3.1: Coherent Optimum Correlator Receiver

3.3 Error Rate Performance (Coherent Case)

With reference to Fig. (3.1), we note that the decision variable $\Lambda_i, i = 1, 2, \ldots, M$ are Gaussian random variables. Let hypothesis H_j be true. Then, the received signal is

given by:

$$r(t) = S_j(t) + n(t), \quad 0 \leq t \leq T \tag{3.6}$$

Then the M decision variables $\Lambda_i, i = 1, 2, \ldots, M$ conditioned on H_1 are given by:

$$\Lambda_{i/H_j} = \int_0^T r(t)\ S_i(t)dt, \quad i = 1, 2, \ldots, M \tag{3.7}$$

Substituting (3.6) in (3.7) we get

$$\Lambda_{i/H_j} = \rho(i,j)E_s + n_{ij}, \quad i = 2, 3, \ldots M \tag{3.8}$$

where

$$\rho(i,j) = \frac{1}{E_s}\int_0^T S_i(t)S_j(t)dt, \quad i = 2, \ldots, M \tag{3.9}$$

and

$$n_{ij} = \int_0^T S_i(t)n(t)dt, \quad i = 1, 2, M \tag{3.10}$$

Given H_j is true, the probability of the receiver making a symbol error is given by:

$$P\left(\in /H_j\right) = P_r\left[\Lambda_1 > \Lambda_j \text{ or } \Lambda_2 > \Lambda_j \ldots \text{ or } \Lambda_M > \Lambda_j/H_j\right] \tag{3.11}$$

Using the identity

$$P\left(x_1 + x_2 + \ldots + x_n\right) \leq \sum_{i=1}^{n} P(x_i) \tag{3.12}$$

we can fit a union bound in (3.11), and it is given by:

$$P(\in /H_j) \leq \sum_{\substack{i=1 \\ i \neq j}}^{M} P_r \left[\Lambda_i > \Lambda_j / H_j\right] \tag{3.13}$$

Averaging over all j, we get:

$$P(\in) = \sum_{j=1}^{M} \sum_{\substack{i=1 \\ i \neq j}}^{M} P(H_j) P_r \left[\Lambda_i > \Lambda_j / H_j\right] \tag{3.14}$$

Assuming all hypothesis are equally likely, the average probability of symbol error can be written as:

$$P(\in) = \frac{1}{M} \sum_{j=1}^{M} \sum_{\substack{i=1 \\ i \neq j}}^{M} \frac{1}{2} \left\{ 1 - erf \left[\sqrt{\frac{E_s}{2N_0} (1 - \rho(i,j))} \right] \right\} \tag{3.15}$$

where $\rho(i,j)$ is as given in (3.9) and

$$erf(x) \triangleq \frac{2}{\sqrt{\pi}} \int_0^x e^{-t^2} dt \tag{3.16}$$

The quantity $\rho(i,j)$ which is required in the evaluation of symbol error rate is the normalized correlation given in (3.9) and a close-form expression for this correlation derived in Appendix A.

Fig. 3.2, shows error rate performances of: i) optimum binary $q = 0.28$ and $w = 1.85$ chirp modulation; ii) BPSK and iii) binary orthogonal FSK. It is noted that optimum binary chirp modulation is superior to binary orthogonal FSK by nearly 2 dB and is poorer to BPSK by 0.8 dB, for error rate $\leq 10^{-6}$. In order to examine the behaviour of binary chirp modulation as a function of modulation parameteres w and q, in Fig. 3.3 we have plotted performance as a function of $w = (1, 1.85, 2, 5)$ for a fixed value of $q = 0.28$. It is observed that as w deviates from the optimum value of 1.85, the error rate performance degrades. The parameter w dictates the bandwidth of the modulated signal. Thus, it is possible to strike trade off between bandwidth

and error rate performance. In Fig. 3.4, we have fixed the value of w and error rate have been plotted for different values of $q = (0.1, 0.28, 0.4, 0.8)$. It is observed that error rate performance is sensitive to variations in q for a fixed value of w.

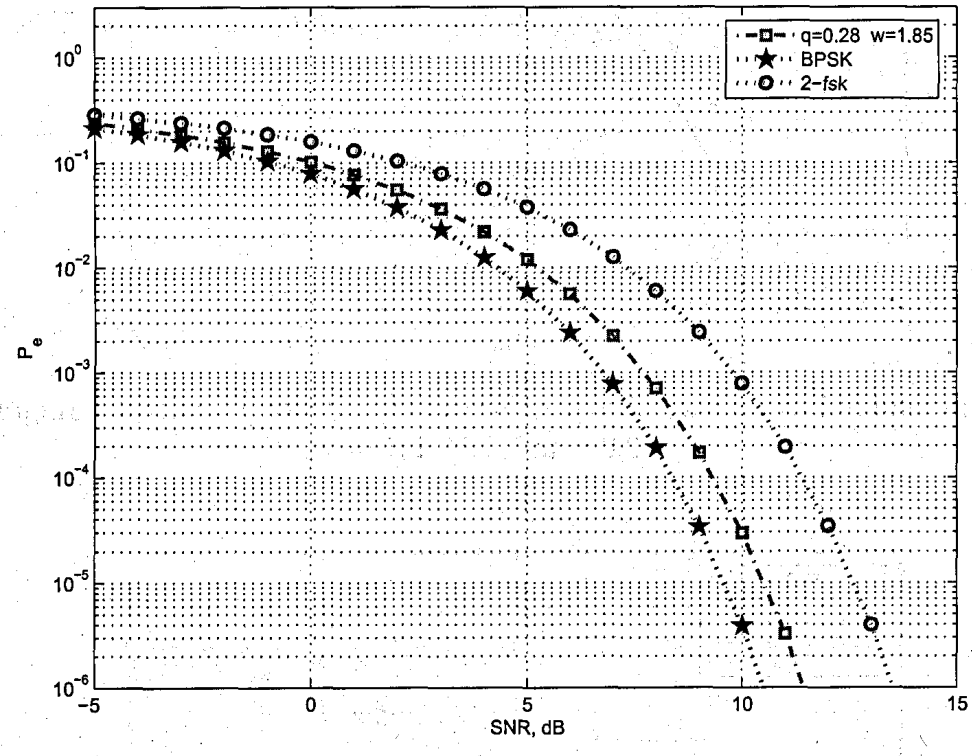

Figure 3.2: Error Probability Performance of Binary Chirp Modulation ($w = 1.85, q = 0.28$)

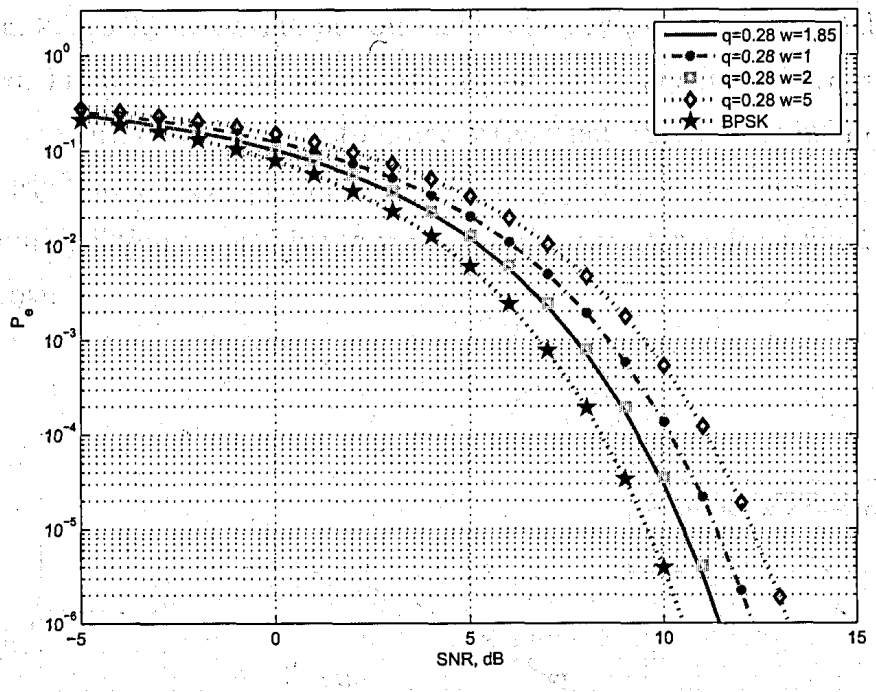

Figure 3.3: Error Probability Performance of Binary Chirp Modulation $(w = 1, 1.85, 2, 5, q = 0.28)$

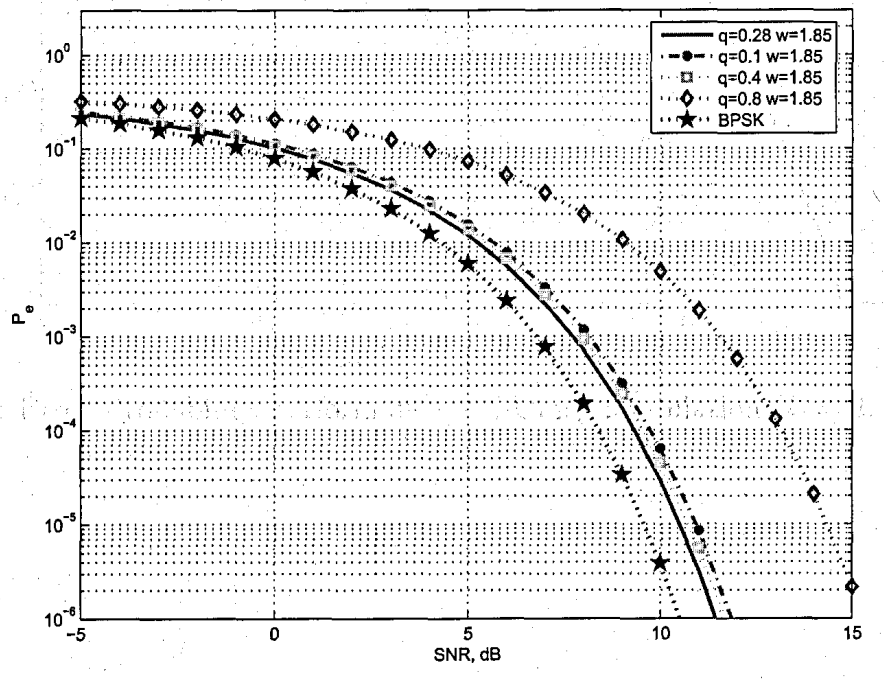

Figure 3.4: Error Probability Performance of Binary Chirp Modulation $(w = 1.85, q = 0.1, 0.28, 0.4, 0.8)$

In Fig. 3.5 to 3.7 error rate performances of 4-ary (w, q) chirp modulation have been plotted. From Fig. 3.5, we note that the optimum 4-ary $(w = 2.4, q = 0.4)$ chirp modulation is marginally superior to 4-ary orthogonal FSK and is inferior to 4-ary PSK by nearly 2 dB. From Fig. 3.6 and 3.7, we note that error rate performance of 4-ary chirp modulation is sensitive to variation of parameter q, for a fixed value of w and vice versa.

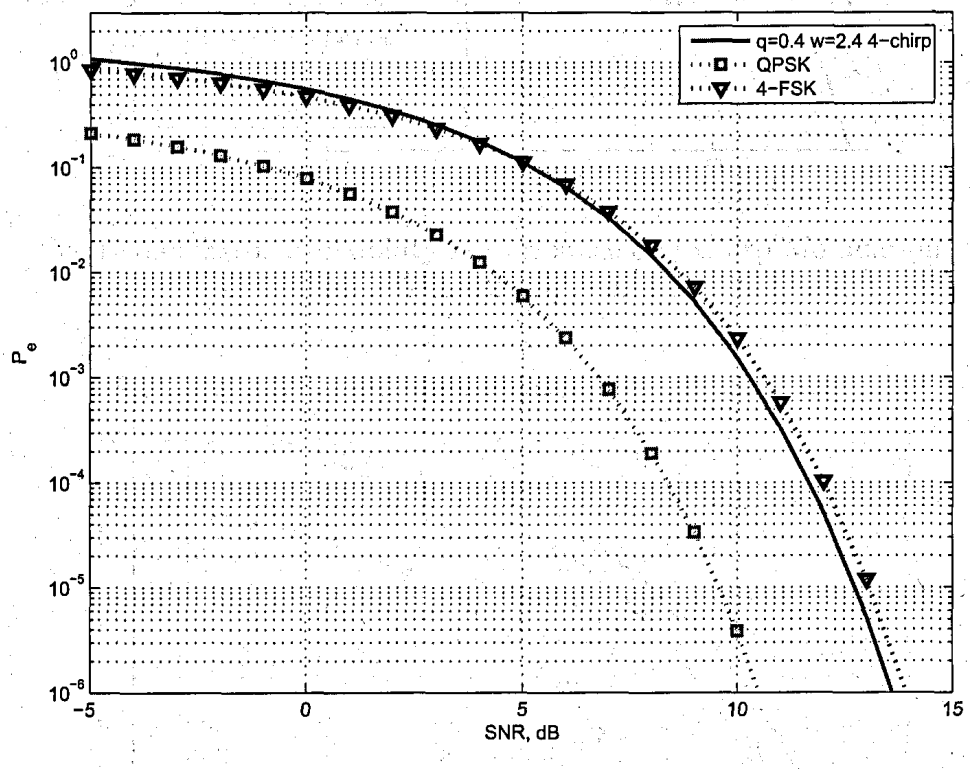

Figure 3.5: Error Probability Performance of 4-Chirp Modulation $(w = 2.4, q = 0.4)$

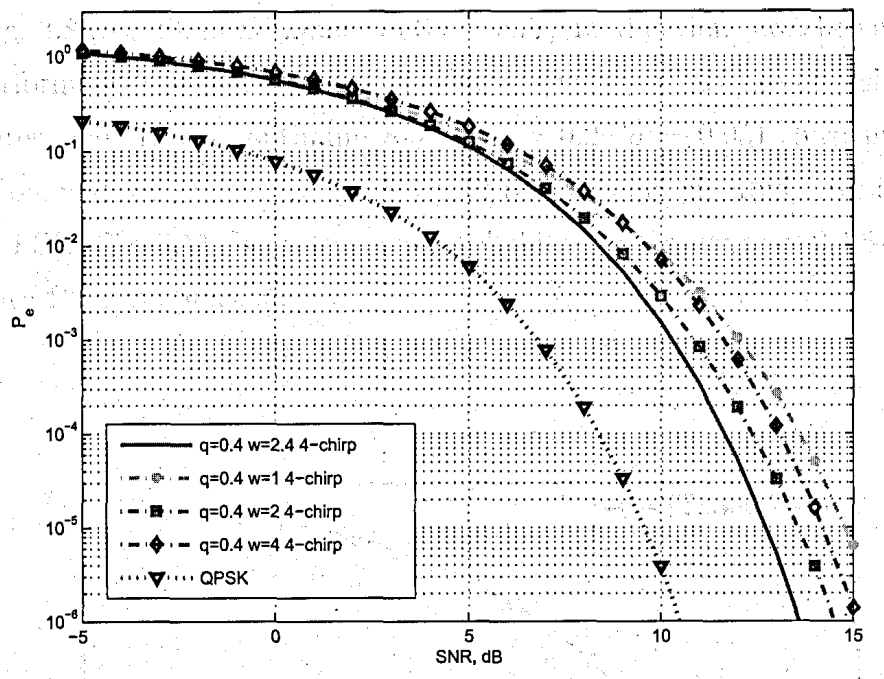

Figure 3.6: Error Probability Performance of 4-Chirp Modulation $(w = 1, 2.4, 2, 4, q = 0.4)$

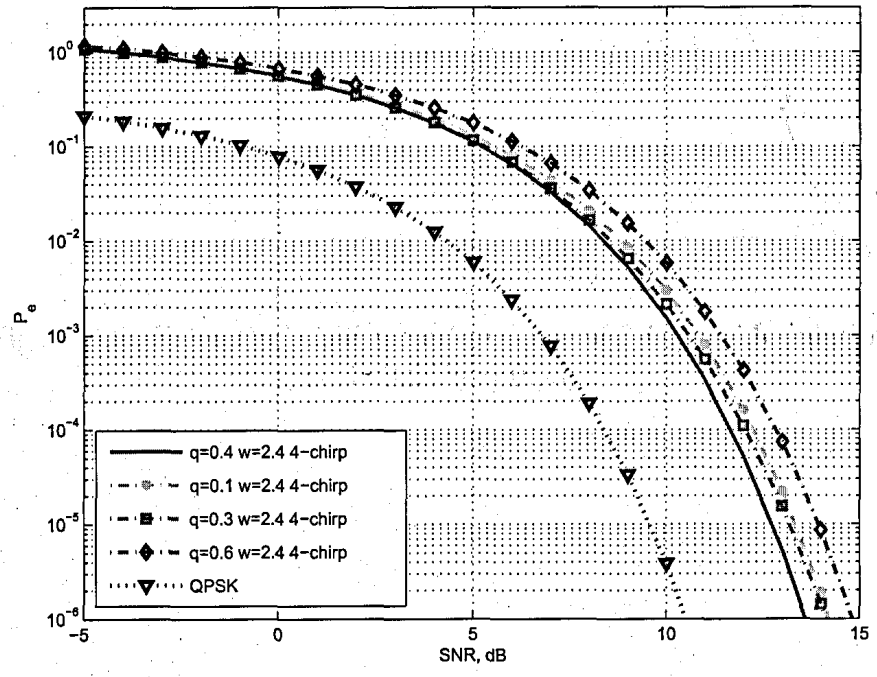

Figure 3.7: Error Probability Performance of 4-Chirp Modulation $(w = 2.4, q = 0.1, 0.3, 0.4, 0.6)$

In Fig. 3.8 to 3.10, performance of 8-ary chirp modulations are shown. In these graphs, performances of 8-ary PSK and 8-ary orthogonal FSK are also shown. For SNRs greater than 11 dB, optimum 8-ary $(w = 0.25, q = 0.95)$ chirp modulation offer the same performance as that of 8-ary PSK and is marginally better than 8-ary orthogonal FSK. Fig. 3.11 shows the error probability performance of 2,4,8-ary Chirp and 2,4,8-ary PSK modulation.

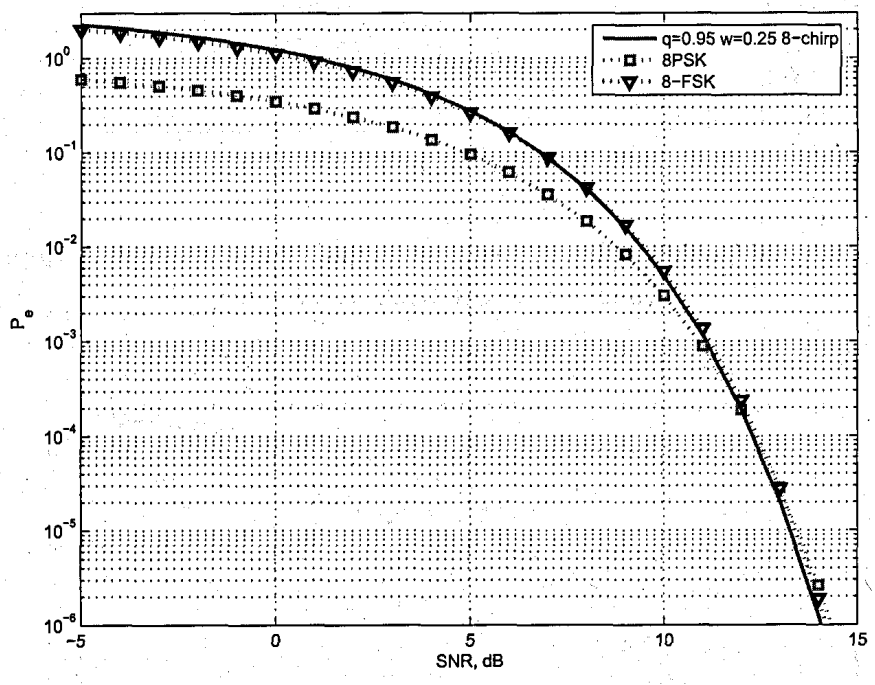

Figure 3.8: Error Probability Performance of 8-Chirp Modulation $(w = 0.25, q = 0.95)$

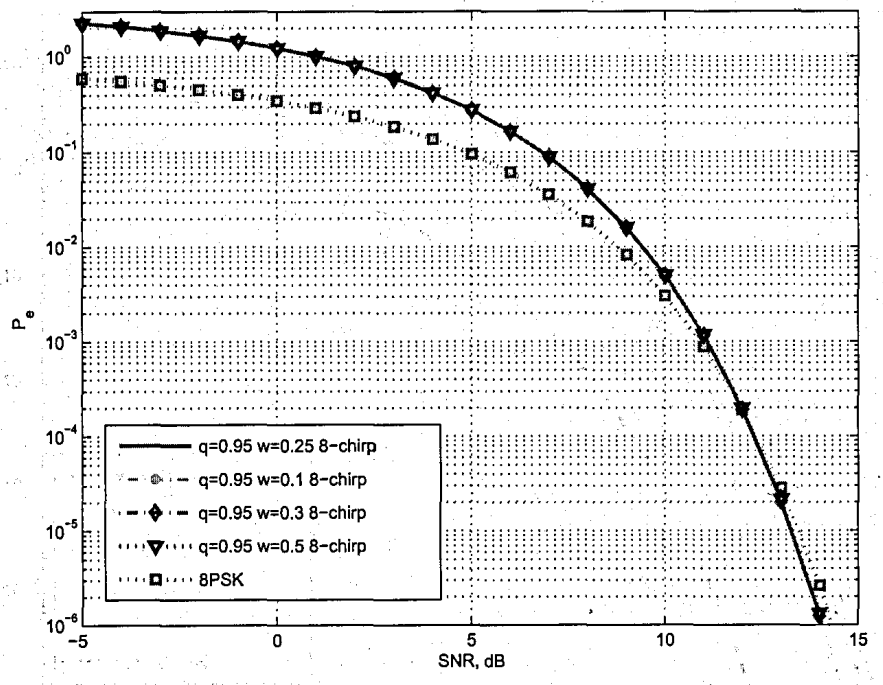

Figure 3.9: Error Probability Performance of 8-Chirp Modulation $(w = 0.1, 0.25, 0.3, 0.5, q = 0.95)$

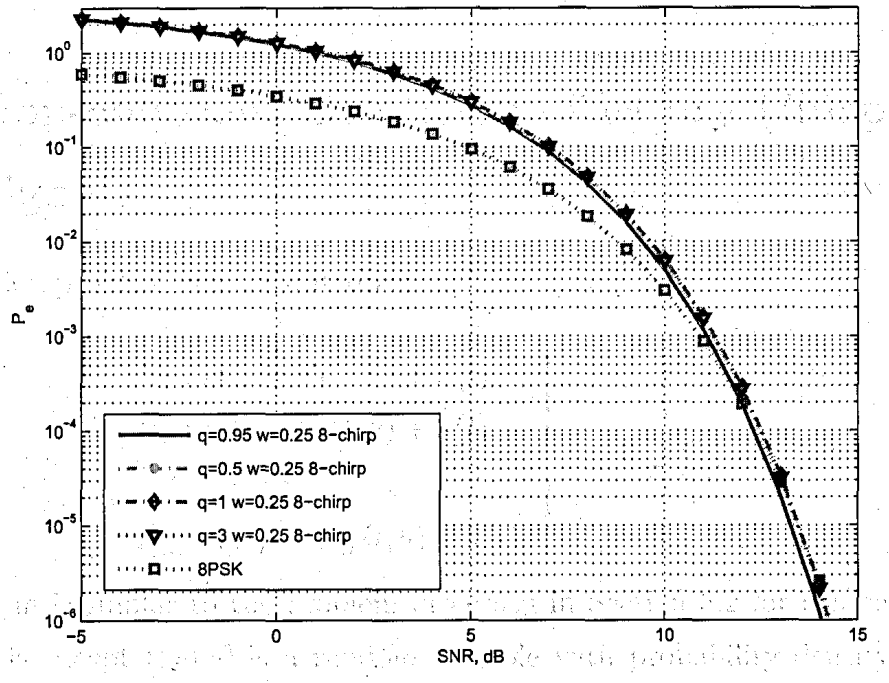

Figure 3.10: Error Probability Performance of 8-Chirp Modulation $(w = 0.25, q = 0.5, 0.95, 1, 3)$

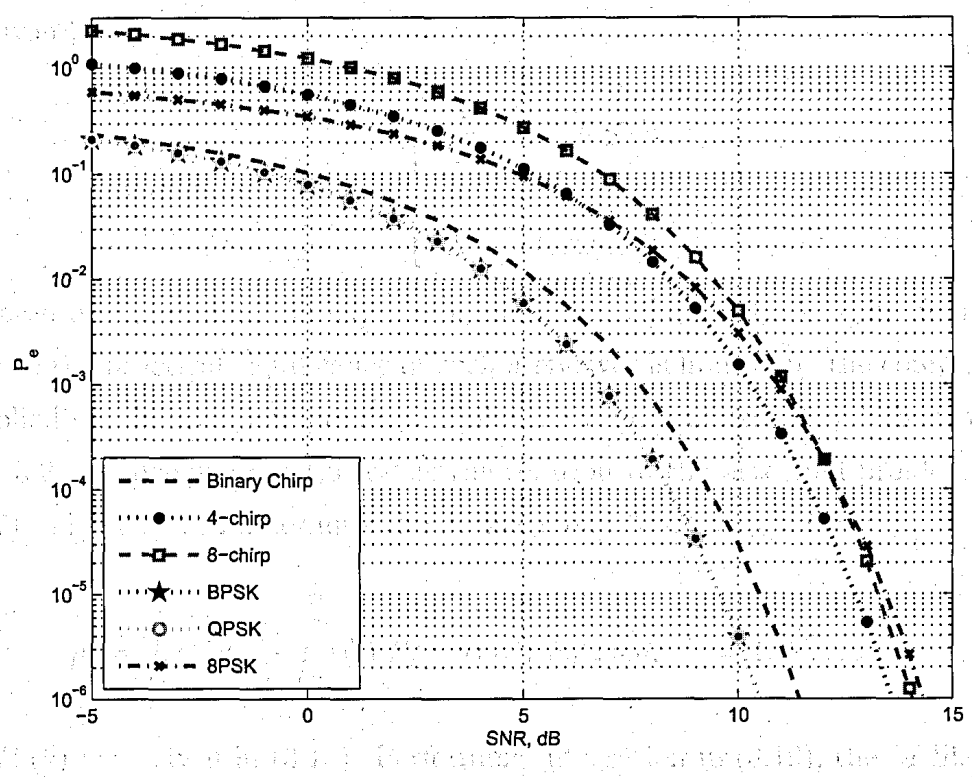

Figure 3.11: Error Probability Performance of 2,4,8-ary Chirp and 2,4,8-ary PSK Modulation

3.4 Non-coherent Detection of M-ary Chirp Signals

The detection problem can be stated as:

$$\left.\begin{aligned} H_1 &: r(t) = S_1(t,\theta) + n(t) \\ H_2 &: r(t) = S_2(t,\theta) + n(t) \\ &\vdots \\ H_M &: r(t) = S_M(t,\theta) + n(t) \end{aligned}\right\} \quad 0 \le t \le T \tag{3.17}$$

This problem is similar to the problem discussed in Section 3.2 for coherent M-ary chirp signals except that θ is a random variable with probability density function

(pdf) given by:

$$P_\theta(\theta) = \begin{cases} \frac{1}{2\pi}, & 0 \leq \theta \leq 2\pi \\ 0, & elsewhere \end{cases} \tag{3.18}$$

In the case of coherent detection, one assumes exact knowledge of θ in the receiver and hence the practical significance of such a receiver is limited by the complexity of the implied synchronization circuitry. Following arguments similar to those used in Section 3.2, the likelihood ratio test is the solution to the detection problem stated in (3.17). This test will determine the M likelihood function given by:

$$\rho_i = \int_\theta \exp(\frac{2}{N_0} \int_0^T r(t)\ S_i(t,\theta)\ dt)\ P_\theta(\theta) d\theta, \quad i = 1, 2, \ldots, M \tag{3.19}$$

where $P_\theta(\theta)$ is as given in (3.18). Performing integration in (3.19), the M likelihood functions can be written as:

$$\rho_i = I_0\left(\frac{2}{N_0} Z_i\right), \quad i = 1, 2, \ldots, M \tag{3.20}$$

where

$$Z_i = \left(\int_0^T r(t)\ S_i(t,0)\ dt\right)^2 + \left(\int_0^T r(t)\ S_i(t,\frac{\pi}{2})\ dt\right)^2 \tag{3.21}$$

and $I_0(.)$ is the modified Bessel function of zero order [20].Since the modified Bessel function is a monotonically increasing function of its argument, the hypothesis test in (3.20) can be carried out using Z_i. Thus, a test equivalent to (3.20) computes the

following M values given by:

$$\Lambda_i = Z_i^2 = \left[\left(\int_0^T r(t)\ S_i(t,0)\ dt \right)^2 + \left(\int_0^T r(t)\ S_i(t,\frac{\pi}{2})\ dt \right)^2 \right]^2, \quad i = 1,2,\ldots,M \tag{3.22}$$

The receiver dictated by (3.22) is shown in Fig. 3.12. Such a receiver is commonly referred as the non-coherent or envelope detector. With reference to Fig. 3.12, the receiver arrives at the optimum decision based on the largest of the M values. Thus, the decision rule is:

$$\Lambda_k = \max\{\Lambda_1, \Lambda_2, \ldots, \Lambda_M\} \tag{3.23}$$

In (3.22), the signals $S_i(t,0)$ and $S_i(t,\frac{\pi}{2})$ for $i = 1,2,\ldots,M$, are given by:

$$S_i(t) = \begin{cases} \sqrt{\frac{2E}{T}} \cos\left(w_c t + i\pi \left\{ h\left(\frac{t}{T}\right) - w\left(\frac{t}{T}\right)^2 \right\} \right), & i \ \ odd \\ \sqrt{\frac{2E}{T}} \cos\left(w_c t - (i-1)\pi \left\{ h\left(\frac{t}{T}\right) - w\left(\frac{t}{T}\right)^2 \right\} \right), & i \ \ even \end{cases} \tag{3.24}$$

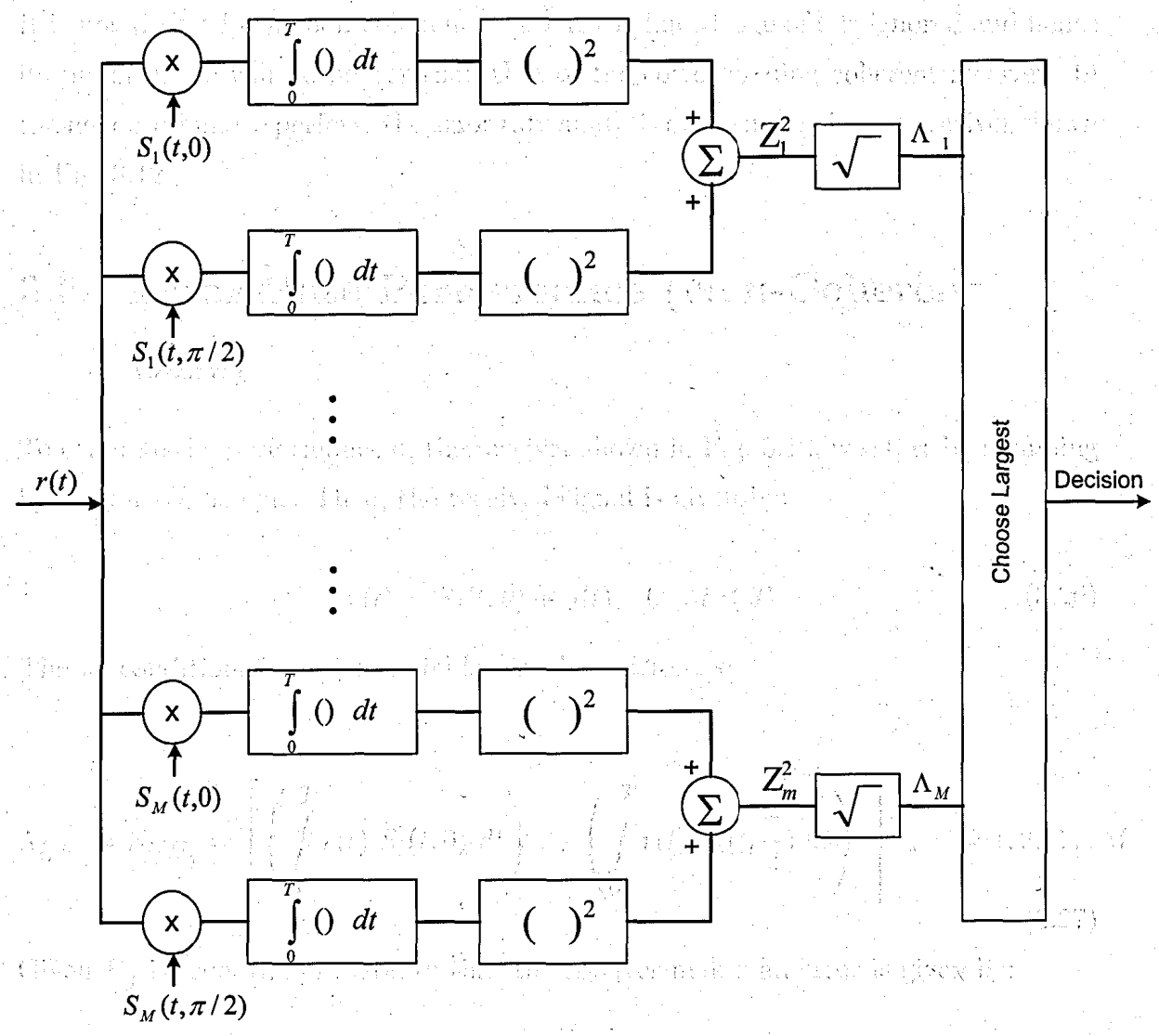

Figure 3.12: Optimum and High-SNR Sub-Optimum Non-Coherent Receiver

and

$$S_i(t,\frac{\pi}{2}) = \begin{cases} \sqrt{\frac{2E}{T}}\sin\left(w_c t + i\pi\left\{h\left(\frac{t}{T}\right) - w\left(\frac{t}{T}\right)^2\right\}\right), & i \ \ odd \\ \sqrt{\frac{2E}{T}}\sin\left(w_c t - (i-1)\pi\left\{h\left(\frac{t}{T}\right) - w\left(\frac{t}{T}\right)^2\right\}\right), & i \ \ even \end{cases} \tag{3.25}$$

It is noted that in the non-coherent receiver, the knowledge of θ is ignored and hence its performance will be poorer than that of the corresponding coherent receiver. In the next section, we perform the error rate analysis of the non-coherent receiver shown in Fig. 3.12.

3.5 Error Rate Performance (Non-Coherent Case)

To evaluate the performance of the receiver shown in Fig. 3.12, we start by assuming hypothesis H_j is true. Then, the received signal is given by:

$$r(t) = S_j(t,\theta) + n(t), \quad 0 \leq t \leq T \tag{3.26}$$

The M conditional decision variables can be written as:

$$\Lambda_{i/h_j} = Z_{i/H_j} = \left[\left(\int_0^T r(t)\ S_i(t,0)\ dt \right)^2 + \left(\int_0^T r(t)\ S_i(t,\frac{\pi}{2})\ dt \right)^2 \right]^2, \quad i = 1,2,\ldots,M \tag{3.27}$$

Given H_j is true, the probability that the receiver makes an error is given by:

$$P\left(\in / H_j\right) = P_r\left[Z_1 > Z_j \text{ or } Z_2 > Z_j \ldots \text{ or } Z_M > Z_j / H_j\right] \tag{3.28}$$

Using (3.12), we get

$$P(\in / H_j) \leq \sum_{\substack{i=1 \\ i \neq j}}^{M} P_r\left[Z_i > Z_j / H_j\right] \tag{3.29}$$

Averaging over all possible symbols, the symbol error rate is given by:

$$P(\in) \leq \frac{1}{M} \sum_{j=1}^{M} \sum_{\substack{i=1 \\ i \neq j}}^{M} P_r\left[Z_i > Z_j / H_j\right] \tag{3.30}$$

In (3.30), we note that Z_i's are Rician random variables. Thus, one Rician random variable exceeding another is given by:

$$P_r\left[Z_i > Z_j/H_j\right] = \frac{1}{2}\left[1 - Q(\sqrt{a},\sqrt{b}) + Q(\sqrt{a},\sqrt{b}))\right] \tag{3.31}$$

where

$$\left\{ \begin{array}{c} a \\ \\ b \end{array} \right\} = \frac{E_s}{2N_0}\left(1 \mp \sqrt{1 - |\rho_c(i,j)|^2}\right) \tag{3.32}$$

and $Q(x,y)$ is the Marcum Q function defined as:

$$Q(x,y) = \int_y^\infty \exp\left[-\left(\frac{x^2+u^2}{2}\right)\right] I_0(xu)\; u\; du \tag{3.33}$$

and the complex correlation $\rho_c(i,j)$ is given by:

$$\rho_c(i,j) = \frac{1}{2E_s}\int_0^T S_i^c(t)\; S_j^{c*}(t)\; dt \tag{3.34}$$

$$S_i^c(t) = \left\{ \begin{array}{ll} \sqrt{\frac{2E}{T}}\; \exp^{j\left[w_c t + i\pi\left\{h\left(\frac{t}{T}\right) - w\left(\frac{t}{T}\right)^2\right\}\right]}, & i\ odd \\ \sqrt{\frac{2E}{T}}\; \exp^{j\left[w_c t - (i-1)\pi\left\{h(\frac{t}{T}) - w(\frac{t}{T})^2\right\}\right]}, & i\ even \end{array} \right. \tag{3.35}$$

and $*$ denotes complex conjugation. A close form expression for $\rho_c(i,j)$ is given in Appendix B.

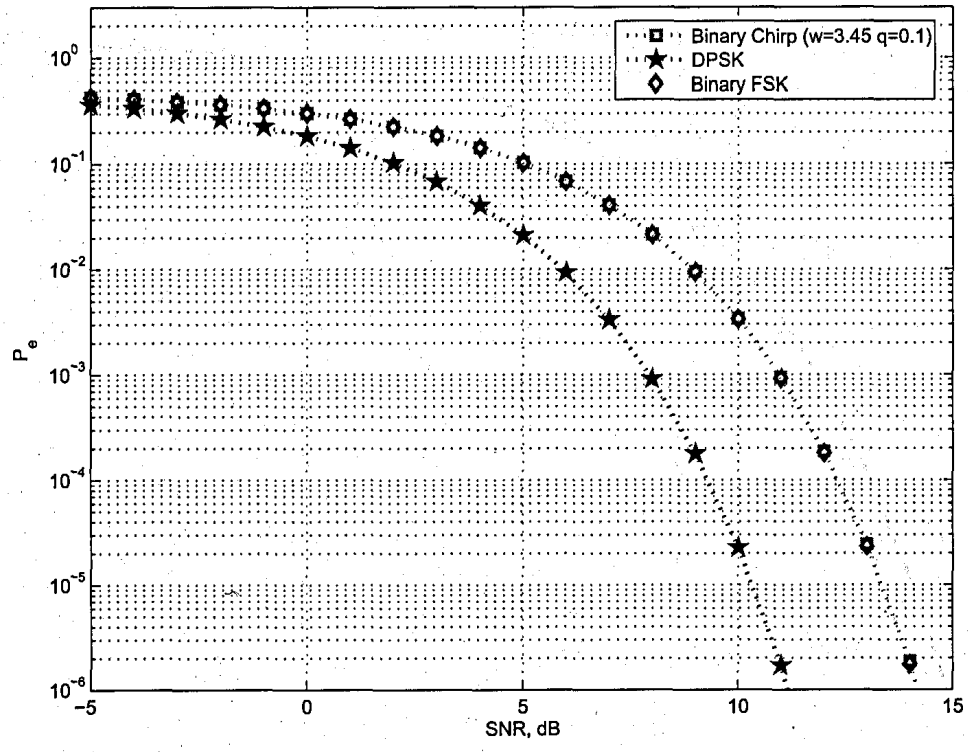

Figure 3.13: Error Probability Performance of optimum $(w = 3.45, q = 0.1)$ 2-ary Chirp, DPSK, and Binary Orthogonal Non-coherent FSK

In Fig. 3.13, the optimum $(w = 3.45, q = 0.05)$ error rate performance for the non-coherent 2-ary chirp has been plotted for different values of SNR. It is noted that the performance of the 2-ary chirp matches the performance of binary orthogonal non-coherent FSK. This is because the optimum error rate performance which occur at $w = 3.45, q = 0.05)$ makes the normalized complex correlation= 0, and thus, performs like orthogonal signals. Also, it can be seen that that the non-coherent 2-ary chirp perform poorer than the conventional Differential Phase Shift Keying (DPSK) by approximately 3.5 dB. In Fig. 3.14, the performance of the 4-ary non-coherent FSK almost identical to the performance of the 4-ary chirp with the same values of w and q.

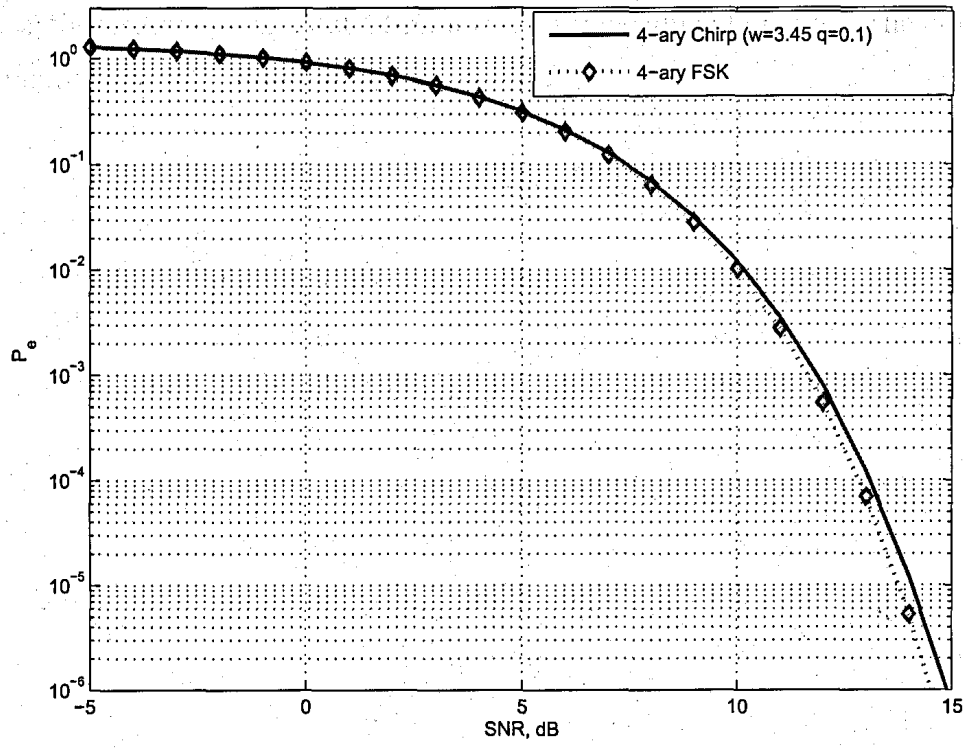

Figure 3.14: Error Probability Performance of $(w = 3.45, q = 0.1)$ 4-ary Chirp, and 4-ary Orthogonal Non-coherent FSK

3.6 Summary

In this Chapter, the detection problem for M-ary chirp signals have been addressed for two cases: Coherent and Non-coherent. In the coherent case, the structure of the optimum correlator receiver has been explained and used to evaluate the error rate performance of M-ary chirp modulation. A comparison between the probability of error of Chirp modulation and other conventional M-ary modulation schemes such as MPSK and MFSK has been provided for $(M = 2, 4, 8)$. It is noted that optimum binary chirp modulation performs better than binary orthogonal FSK by approximately 2 dB and is poorer than BPSK by nearly 0.8 dB. For $M = 4$, the optimum 4-ary $(w = 2.4, q = 0.4)$ chirp modulation performs better than 4-ary orthogonal FSK and when $M = 8$, chirp modulation has performance same as 8-ary FSK. In the non-coherent case, optimum 2-ary $(w = 3.45, q = 0.05)$ offer the same performance

as 2-ary orthogonal non-coherent FSK. For the same value of w and q, the 4-ary FSK is marginally superior to the 4-ary chirp.

Chapter 4
Coherent Detection of MCPCM Signals in Gaussian Noise

4.1 MCPCM Signalling

In an MCPCM system, the general expression for the transmitted signal is given by

$$S(t,\tilde{a}) = \sqrt{2S}\cos(2\pi f_c t + \phi(t,\tilde{a}) + \phi_0), \quad -\infty < t < +\infty \tag{4.1}$$

where the information bearing phase is given by

$$\phi(t,\tilde{a}) = \int_{-\infty}^{t} \sum_{i=-\infty}^{\infty} a_i g(x - iT)\, dx, \quad -\infty < t < +\infty \tag{4.2}$$

and

$$\tilde{a} = \ldots, a_{-2}, a_{-1}, a_0, a_{+1}, a_{+2}, \ldots \tag{4.3}$$

is an infinitely long sequence of un-correlated M-ary data symbols, each assuming one of the values

$$a_i = \pm 1, \pm 3, \pm 5, \ldots, \pm(M-1); \quad i = 0, \pm 1, \pm 2, \ldots \tag{4.4}$$

with probability

$$P(a_i) = \frac{1}{M}; \quad i = 0, \pm 1, \pm 2, \ldots \tag{4.5}$$

In (4.1), $S = \left(\frac{E_s}{T}\right)$ is the symbol power, f_c is the carrier frequency, T is the symbol duration, and ϕ_0 is the arbitrary phase shift, which without loss of generality can be set to zero for a coherent system. In (4.2), the baseband phase function is defined by:

$$q(t) = \int_{-\infty}^{t} g(x)dx \tag{4.6}$$

the information carrying the phase can be written as:

$$\phi(t, \tilde{a}) = \sum_{i=-\infty}^{\infty} a_i q(t - iT) \tag{4.7}$$

For the full-response system, data symbol affects the instantaneous frequency only over one data symbol. Thus, for chirp signals, the phase function $q(t)$ is given by

$$q(t) = \begin{cases} 0, & t \leq 0, \quad t>T \\ 2\pi \int_0^t g(x)dx, & 0 \leq t \leq T \\ \pi q = \pi(h - w), & t = T \end{cases} \tag{4.8}$$

where the instantaneous frequency deviation for the MCPCM signal is given by:

$$g(t) = \begin{cases} 0, & t \leq 0, \quad t>T \\ \frac{h}{2T} - \frac{w}{T^2}\, t, & 0 \leq t \leq T \end{cases} \tag{4.9}$$

Thereby, the phase function is given by

$$q(t) = \begin{cases} 0, & t \leq 0, \quad t>T \\ \pi\left\{h\left(\frac{t}{T}\right) - w\left(\frac{t}{T}\right)^2\right\}, & 0 \leq t \leq T \\ \pi q = \pi(h - w), & t = T \end{cases} \tag{4.10}$$

Where h, w, and q are dimensionless modulation parameters. Of these, h represents the initial peak-to-peak frequency deviation divided by the symbol rate $1/T$, w denotes the frequency sweep width divided by the symbol rate. Since $h = q + w$, we choose q and w to be the independent signal parameters to describe a given MCPCM system. The accumulated excess phase due to the kth data symbol at the end of

the kth data symbol interval is equal to $p\pi q$, $p = \pm 1, \pm 3, \ldots, \pm M$ depending upon $a_k = \pm 1, \pm 3, \ldots, \pm M$. It is noted that CPFSK is a subclass of MCPCM with $w = 0$.

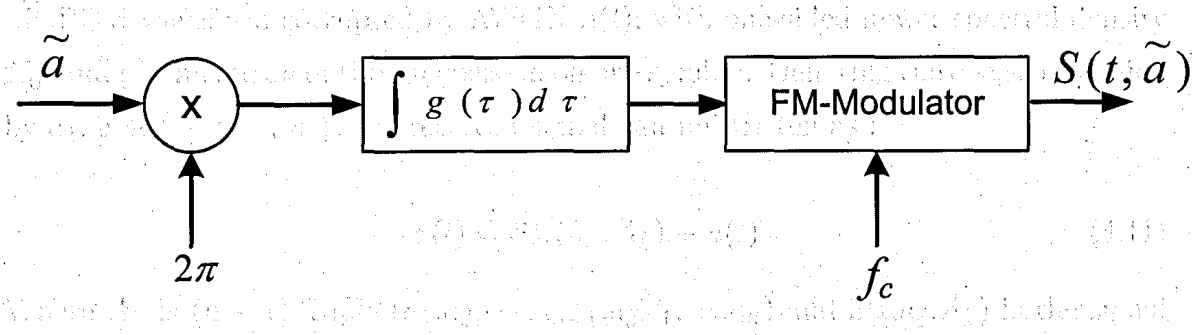

Figure 4.1: Schematic Modulator for CPC System

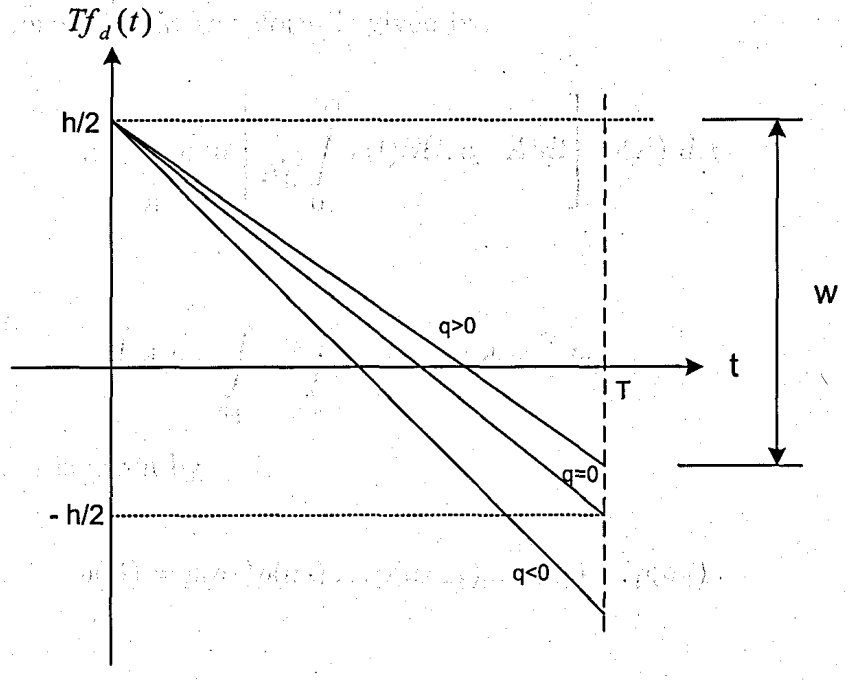

Figure 4.2: Instantaneous Frequency Deviation in CPC Signalling

In Fig. 4.1 a schematic modulator for generality CPC signals is shown. In Fig. 4.2, the parameters h and w are illustrated. The possible phase trajectories, using the phase term of (4.2), for binary and quaternary modulations are shown in Fig. 2.6 and Fig. 2.7 , respectively.

4.2 Optimum Coherent Maximum Likelihood MCPCM Receiver

The detection problem addressed here consists of observing n symbol intervals of MCPCM waveform corrupted by AWGN $n(t)$, with one-sided power spectral density N_0, and producing an optimum decision on one symbol. Denoting the decesion symbol by a_δ, $\delta \in \{ 1,2,\ldots, n \}$, the received signal can be written as :

$$r(t) = S(t, a_\delta, A_k) + n(t) \tag{4.11}$$

Where A_k is $(n-1)$-Tuple $(a_1,a_2,\cdots,a_{\delta-1},a_{\delta+1},\ldots,a_n)$ and S(t,a_δ,A_k) is the signal waveform over n symbol interval. The detection problem in (4.11) is the M-ary composite hypothesis testing problem [30] and the solution is given by the likelihood ratio test and for MCPCM waveform is given by:

$$\Lambda_i = \int_A \exp\left[\frac{2}{N_0}\int_0^{nT} r(t)S(t, a_\delta, A)dt\right] p(A)\, dA \tag{4.12}$$

Where

$$\int_A dA = \int_{a_1} \ldots \int_{a_n} \ldots da_1 \ldots da_{\delta-1} da_{\delta+1} \ldots \tag{4.13}$$

The density of A is given by

$$p(A) = p(a_1)p(a_2)\ldots p(a_{\delta-1})p(a_{\delta+1})\ldots p(a_n) \tag{4.14}$$

and

$$p(a_i) = \frac{1}{M}\left[\delta(a_{i-1}) + \ldots + \delta(a_i + (n-1))\right] \tag{4.15}$$

Substituting (4.13)-(4.15) in (4.12), we obtain the Mlikelihood functions given by:

$$\begin{aligned}\Lambda_1 &= \frac{1}{m}\sum \exp\left[\frac{2}{N_0}\int_0^{nT} r(t)\ S(t, a_\delta = +1, A_k)\ dt\right] \\ &\vdots \\ \Lambda_M &= \frac{1}{m}\sum \exp\left[\frac{2}{N_0}\int_0^{nT} r(t)\ S(t, a_\delta = -(M-1), A_k)\ dt\right]\end{aligned} \tag{4.16}$$

Where $m = M^{n-1}$. The maximum likelihood receiver produce an estimate $\tilde{a}_\delta$ of a_δ using

$$a_\delta = \begin{cases} p, & p\ odd \\ -(p-1), & p\ even \end{cases} \tag{4.17}$$

Where $1 \leq p \leq M$ and correspond to λ_p such that

$$\lambda_p = max\{\lambda_i; i = 1, 2, \ldots, M\} \tag{4.18}$$

for some p. The structure of the optimum coherent receiver is shown in Fig. 4.3. This receiver essentially correlates the received waveform with each of the m possible transmitted signals with the data in the decision interval $a_\delta = +1$, then forms the sum of $\exp(C_j)$, where C_j is the correlation of the received waveform with the jth signal waveform with a data $+1$ in the decision interval. Similar operation of correlating and summing for each set of the m possible waveforms with decision interval data $\pm 1, \pm 3, \ldots, \pm(m-1)$ are performed and the decision is based on the largest of M sums obtained. Since the evaluation of exact error rate of this receiver is too complex, bounds on its error rate performance that are tight at high SNR can be determined. This is carried out in the next section.

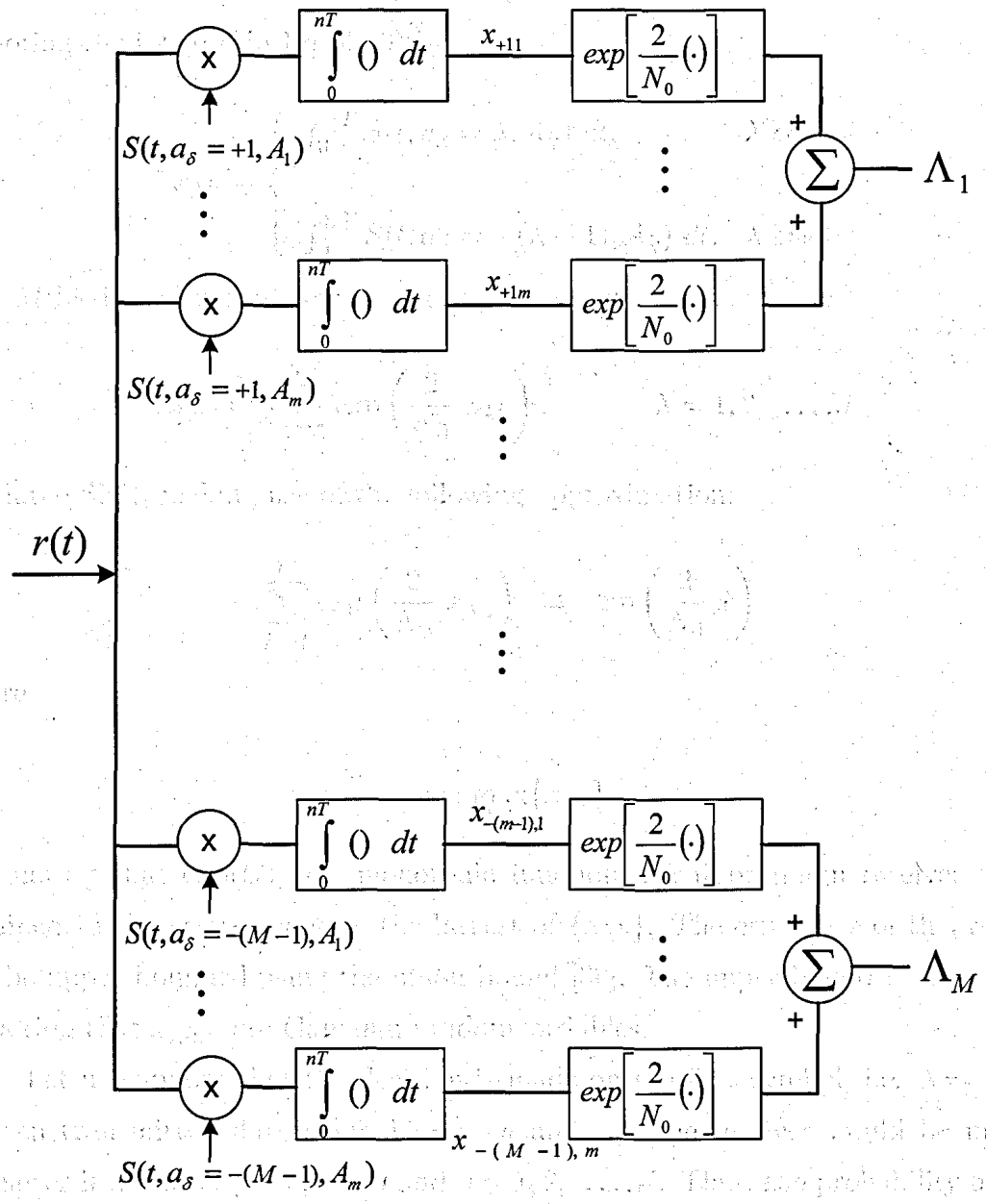

Figure 4.3: Optimum and High-SNR Sub-optimum MCPCM Receiver

4.3 Performance of The Optimum MCPCM Receiver

Denoting the integral in Eq (4.16) by:

$$x_{\lambda k} = \begin{cases} \int_0^{nT} S(t, a_\delta = \lambda, A_k)\, dt, & \lambda \text{ odd} \\ \int_0^{nT} S(t, a_\delta = -(\lambda - 1), A_k)\, dt, & \lambda \text{ even} \end{cases} \tag{4.19}$$

The M likelihood parameters can be expressed as:

$$\Lambda_\lambda = \frac{1}{m} \sum_{k=1}^{m} \exp\left(\frac{2}{N_0}\, x_{\lambda k}\right), \qquad \lambda = 1, 2, \ldots, M \tag{4.20}$$

For large SNR, making use of the following approximation:

$$\sum_{k=1}^{m} \exp\left(\frac{2}{N_0}\, x_{\lambda k}\right) \cong \exp\left(\frac{2}{N_0}\, \tilde{x}\right) \tag{4.21}$$

where

$$\tilde{x} = \max_{\lambda, k}\{x_{\lambda k}\} \tag{4.22}$$

and noting that $\exp(C)$ is a monotonic function, a sub-optimum receiver can be obtained. This receiver chooses the largest of $\{x_{\lambda k}\}$. The error rate of this receiver can be upper bounded using the union bound [30]. The upper bound is constructed by noting that $x_{\lambda k}$ s are Gaussian random variables.

Let us suppose that the decision is made on the first symbol, i.e. $\lambda = 1$. For a given transmitted data symbol $a_1 = u$ and A_k, the receiver would be in error whenever it decides $a_1 = v, v \neq u$ and $v = 1, 2, \ldots, M$. Thus, the probability of error is given by:

$$P_r[a_1 \neq u / a_1 = u, A_k] \leq \sum_{\substack{v=1 \\ v \neq u}}^{M} \sum_{j=1}^{m} P_r[x_{vj} > x_{uk}] \tag{4.23}$$

Averaging over all possible equally likely a_k, the expression for error probability in (4.23) can be written as:

$$P_r\left[a_1 \neq u/a_1 = u, A_k\right] \leq \sum_{\substack{v=1 \\ v\neq u}}^{M} \sum_{j=1}^{m} \sum_{k=1}^{m} P_r\left[x_{vj} > x_{uk}\right] \tag{4.24}$$

The overall probability of an error may then be obtained by averaging (4.24) over all possible input data symbols, i.e.

$$P_{e,M} \leq \frac{1}{mM} \sum_{u=1}^{M} \sum_{\substack{v=1 \\ v\neq u}}^{M} \sum_{j=1}^{m} \sum_{k=1}^{m} P_r\left[x_{vj} > x_{uk}\right] \tag{4.25}$$

Where the probability for one Gaussian random variable exceeding another is given by:

$$P_r\left[x_{vj} > x_{uk}\right] \leq Q\left[\sqrt{\frac{nE_s}{N_0}(1-\rho(vj,uk))}\right] \tag{4.26}$$

and

$$\rho(vj,uk) = \frac{1}{nE_s} \int_0^{nT} S(t, a_1 = v, A_j) S(t, a_1 = u, A_k) dt \tag{4.27}$$

is the normalized correlation between the signals $S(t, a_1 = v, A_j)$ and $S(t, a_1 = u, A_k)$. To facilitate error probability comparisons with other modulation, we normalize the symbol energy to bit energy using

$$E_s = E_b \log_2 M \tag{4.28}$$

Although, an explicit expression given by (4.25) was obtained for upper bound on the performance of the optimum receiver, the computation required for evaluating this expression is too large. However, the number of computations can be reduced by averaging (4.25)-(4.27), i.e. by recognizing and identifying the Gaussian pairs which

have the same correlation. Thus, an expression equivalent to (4.25) is given by:

$$P_{e,M} < (M-1)M^{n-1} \int_{\tilde{\gamma}} Q\left[\sqrt{\frac{nE_s}{N_0}(1-\xi(\tilde{\gamma}))}\right] p(\tilde{\gamma})\, d\tilde{\gamma} \tag{4.29}$$

where

$$\int_{\tilde{\gamma}} d\tilde{\gamma} = \int \dots \int d\gamma_1 d\gamma_2 \dots d\gamma_n \tag{4.30}$$

and

$$p(\tilde{\gamma}) = p(\gamma_1) \dots p(\gamma_n) \tag{4.31}$$

with

$$p(\gamma_1) = \frac{1}{M(m-1)} \sum_{j=1}^{M-1} j\,[\delta(\gamma_1 + 2(m-j)) + \delta(\gamma_1 - 2(m-j))] \tag{4.32}$$

and

$$p(\gamma_1) = \frac{1}{M}\gamma_i + \frac{1}{M^2} \sum_{j=1}^{M} j\,[\delta(\gamma_1 + 2(m-j)) + \delta(\gamma_1 - 2(m-j))] \tag{4.33}$$

In (4.29), $\xi(\tilde{\gamma})$ is related to the correlation function via

$$\rho(vj, uk) = \xi(\tilde{\gamma}) \tag{4.34}$$

where $\tilde{\gamma} = (\gamma_1, \gamma_2, \dots, \gamma_n)$ is the difference sequence between data symbols of the sequence (v, A_j) and data symbols of sequence (u, A_k). For M-ary data γ_1 takes values from the set $\{\pm 2, \pm 4, \dots, \pm 2(m-1)\}$ and $\gamma_i, i = 1, 2, 3, \dots, n$ from the set $\{0, \pm 2, \pm 4, \dots, \pm 2(m-1)\}$. Using the expression for the sequence correlation given

by (4.34) in (4.24) for the error probability, one would require less computation than by using (4.26) and (4.27).

4.4 Distance Properties of MCPCM Signals

The distance between waveforms is a key concept [30] in understanding the ultimate utility of any arbitrary signaling scheme in digital communications. With reference to the set of MCPCM waveforms of duration n symbol intervals available to the transmitter, the Euclidean squared distance between signals $S(t, a_1 = v, A_j)$ and $S(t, a_1 = u, A_k)$ is given by:

$$D_n^2(vj, uk) = \int_0^{nT} \left| S(t, a_1 = v, A_j) - S(t, a_1 = u, A_k) \right|^2 dt \tag{4.35}$$

It can be shown that (4.35) reduces to:

$$D_n^2(vj, uk) = 2E_s \left[n - \sum_{i=1}^{n} \frac{1}{T} \int_0^T cos(\Delta\phi_i(t, vj, uk))\, dt \right] \tag{4.36}$$

where

$$\Delta\phi_i(t, vj, uk) = (a_i^j - a_i^k) q(t - (i-1)T) + \theta_{i-1} \tag{4.37}$$

with

$$\theta_{i-1} = \pi q \sum_{r=1}^{i-1} (a_r^j - a_r^k) \tag{4.38}$$

In (4.37), $q(t)$ is the phase function for MCPCM signals. The quantity $\Delta\phi_i(t, vj, uk)$ represents the phase difference between the signals $S(t, a_1 = v, A_j)$ and $S(t, a_1 = u, A_k)$ during the ith symbol interval. For sufficiently large SNR, the performance of

the optimum receiver is nominated by a parameter know as the Minimum Euclidean Distance [2]. Defined as:

$$D^2_{min,n} = \min_{\substack{v,u,j,k \\ v \neq u}} \{D^2_n(vj, uk)\} \tag{4.39}$$

and the performance then is approximately given by:

$$P_e \simeq Q\left[\sqrt{\frac{D^2_{min,n}}{2N_0}}\right] \tag{4.40}$$

using energy normalization, the normalized squared Euclidean distance is expressed as:

$$d^2 = \frac{D^2_n}{2E_b} \tag{4.41}$$

By using this normalization, we can compare different M-ary schemes on an equal $\frac{E_b}{N_0}$ basis. As a reference point, we note that $d^2_{min} = 2$, for BPSK, QPSK, and MSK. An estimate of the SNR gain relative to BPSK is then obtained using:

$$G_n = 10\log_{10}\left[\frac{d^2_n}{2}\right] \tag{4.42}$$

For MCPCM, (4.36) can be shown to be given by:

$$\begin{aligned} D^2_n(\tilde{\gamma}) &= D^2_n(vj, uk) \\ &= 2E_s\{n - \textstyle\sum_{i=1}^{n} \frac{1}{\sqrt{2|\gamma_i|w}} [\cos(\Omega_i)(C(H_{2i}) + C(H_{1i})) + \sin(\Omega_i)(S(H_{2i}) + S(H_{1i}))]\} \end{aligned} \tag{4.43}$$

where

$$\Omega_i = \left[\frac{\pi}{2}\frac{(w+q)^2}{2w}|\gamma_i| + 2q\ sgn(\gamma_i)\sum_{r=1}^{i-1}\gamma_r\right] \tag{4.44}$$

$$H_{2i} = \sqrt{\frac{|\gamma_i|}{2w}}(w - q) \tag{4.45}$$

$$H_{1i} = \sqrt{\frac{|\gamma_i|}{2w}}(w+q) \tag{4.46}$$

$$sgn(x) = \begin{cases} +1, & x \geq 0 \\ -1, & x < 0 \end{cases} \tag{4.47}$$

$$C(x) = \int_0^x \cos(\pi y^2/2)\, dy \tag{4.48}$$

$$S(x) = \int_0^x \sin(\pi y^2/2)\, dy \tag{4.49}$$

$$\gamma_i = a_i^j - a_i^k, i = 1, 2, \ldots, n \tag{4.50}$$

For the MCPCM signals, to determine $D^2_{min,n}$, we just need to consider $\gamma_i \in \{0, \pm 1, \pm 2, \ldots, \pm 2(M-1)\}$ and $\gamma_1 \in \{2, 4, 6, \ldots, 2(m-1)\}$

An important tool in the analysis of the distance properties associated with the MCPCM signals is its phase tree. To calculate the maximum squared Euclidean distance associated with MCPCM signalling set, with signals in that set defined over n symbol intervals, all pairs of phase trajectories in the phase tree over n symbol intervals must be considered. The phase trajectories over the first symbol interval, however, must not coincide. The squared Euclidean distance is then determined using (4.36) for all these pairs, and the maximum is the derived result of (4.39). Using the fact, that the Euclidean distance is a non-decreasing function of observation length n, an upper bound for all n, may be obtained by considering just a few representative pairs of infinitely long sequences. Good candidates for all these sequences are pairs that merge as soon as possible. It is seen that such infinitely long sequence is:

$$\tilde{\gamma} = +x_1, -x_1, 0, 0, \ldots \tag{4.51}$$

with $x_1 = 2, 4, 6, \ldots, 2(m-1)$. Using (4.51), an upper bound on the maximum Euclidean squared distance for MCPCM is given by:

$$d^2_{B,M}(w,q) = \log_2 M \min_{1\le p\le M-1}\{2 - \frac{\cos(p\pi q)}{\sqrt{pw}}[\cos(\frac{\pi p(w^2+q^2)}{2w})(C(x)+C(y))+$$

$$\sin(\frac{\pi p(w^2+q^2)}{2w})(S(x)+S(y))]\} \tag{4.52}$$

where $x = \sqrt{\frac{p}{w}}(w-q)$ and $y = \sqrt{\frac{p}{w}}(w+q)$. It is noted that

$$d^2_{B,M}(w,q) = d^2_{B,M}(w,-q) = d^2_{B,M}(w,|q|) \tag{4.53}$$

Since the upper bound of (4.52) is a function of the set of signal modulation parameters (w,q), to find a tighter bound on G_n inherent in MCPCM signals, $d^2_{B,M}$ was computed in the signal space by $0 < q \le 2$ *and* $0 < w \le 10$. The results of the computation are shown in Table 4.1, where (w,q) that maximized $d^2_{B,M}$are shown for M=2,4,8, and 16 . The global maxima give an idea of the limiting gains available with MCPCM. For example, 4-ary MCPCM will offer an advantage of 4.67 dB, at best, relative to PSK. However, it should be noted that the actual value of d^2_n will always be smaller than the global maximum of its bound. That is to say for $q \neq 0$, a value of D^2_n close to maximum may be found out.

M	(w,q)	max $\{d^2_{B,M}\}$	G_n, dB
2	(2.4,0.0)	2.93	1.66
4	(0.8,0.0)	5.86	4.67
8	(0.6,0.0)	8.79	6.43
16	(0.6,0.0)	11.72	7.68

Table 4.1: (w,q) maximizing $d^2_{B,M}$

Tables 4.2 to 4.4 show sets of (w, q) that maximize d_n^2 , computed using (4.41), in the modulation parameter space $0 < q \leq 2$ and $0 < w \leq 10$ for $M = 2, 4, 8$ and observation intervals of 2,3,4, and 5. It is observed that the 2-ary $(w = 2.36, q = 0.12)$ MCPCM system provides a gain that is only 8% less than the best 2-ary MCPCM system which has a limiting advantage of 1.66 dB. On the other hand, 4-ary and 8-ary MCPCM systems with 5 symbol observations provide gains that are nearly 75% and 70% of their respective best systems. This shows that an observation interval longer than 5 symbols may be used to obtain further advantage in SNR gains. However, it is noted that this may not be true when one chooses a different parameter space.

n	(w,q)	max $\{d_n^2\}$	G_n, dB
2	(1.55,0.25)	2.571	1.09
3	(2.36,0.192)	2.744	1.42
4	(2.40,0.156)	2.827	1.50
5	(2.40,0.140)	2.847	1.53
6	(2.36,0.120)	2.868	1.57

Table 4.2: Optimum (w, q) maximizing d_n^2 for 2-ary MCPCM

n	(w,q)	max $\{d_n^2\}$	G_n, dB
2	(2.94,0.20)	3.689	2.66
3	(2.55,0.41)	4.416	3.44
4	(2.54,0.39)	4.417	3.44
5	(2.54,0.39)	4.417	3.44

Table 4.3: Optimum (w, q) maximizing d_n^2 for 4-ary MCPCM

n	(w, q)	max $\{d_n^2\}$	G_n, dB
2	(4.67,0.88)	4.712	3.72
3	(4.50,0.90)	5.084	4.05
4	(4.89,0.90)	5.476	4.37
5	(4.93,0.90)	5.653	4.51

Table 4.4: Optimum (w, q) maximizing d_n^2 for 8-ary MCPCM

4.5 Numerical Results on Error Probability Bounds

In the previous section we obtained some insight into the distance properties associated with MCPCM systems using the minimum distance criterion, wherein a set (q, w), for a given M and observation interval n, was chosen that maximized the minimum distance between pairs of signals in the signalling set. Alternatively, in this section, we examine the MCPCM systems using minimum probability of error criterion. That is, we examine MCPCM systems that minimize the error probability upper bound on the performance of the optimum receiver.

The error probability upper bound of (4.25) is a function of: i) Signal-to-Noise Ratio, E_b/N_0 ; ii) number of observation intervals,n ; iii) the signal modulation parameters, (w, q) ; and iv) the number of levels of the input alphabet, M. For a given M, n and a suitably high SNR, the modulation parameter set (w, q) that should be chosen is the one that minimizes the error probability upper bound of (4.25). The optimum (w, q)s have been determined at SNRs of 6, 8, and 10 dB, for $2 \leq n \leq 5$ and $M = 4$ and 8. The signal parameter space is bounded by $0 < q \leq 2$ and $0 < w \leq 10$. The probability of error curve of the optimum (w, q) for observation interval of $n = 5$ is illustrated in Fig. 4.4 to Fig. 4.6 for $M = 2, 4$, and 8. The optimum sets thus obtained are tabulated in Tables 4.5 to 4.7, for 2-, 4-, and 8-ary MCPCM.

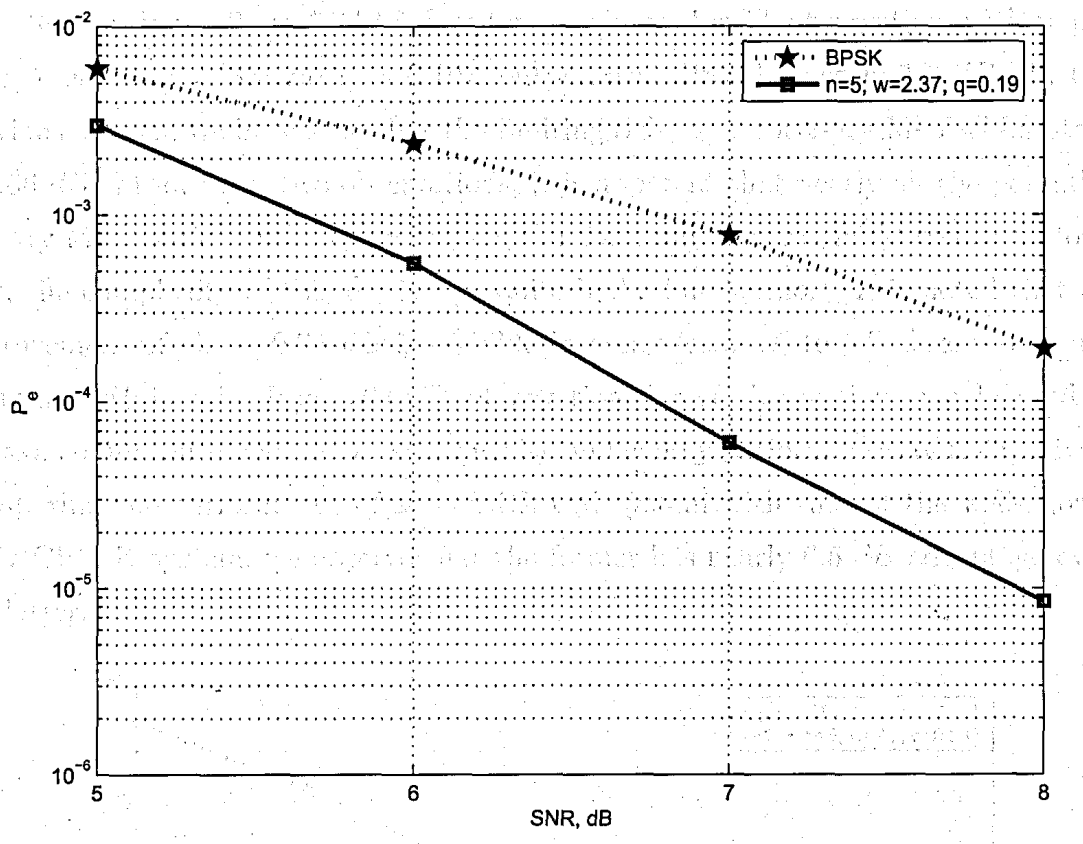

Figure 4.4: Optimum Error Probability Performance of 2-ary Chirp $(w = 2.37, q = 0.19)$ and $n = 5$ with BPSK Modulation

SNR \ n	2	3	4	5
6	(1.85,0.28) 1.23×10^{-3}	(2.06,0.24) 6.46×10^{-4}	(2.22,0.23) 4.24×10^{-4}	(2.33,0.22) 3.55×10^{-4}
8	(1.88,0.27) 4.92×10^{-5}	(2.16,0.23) 1.70×10^{-5}	(2.33,0.21) 1.00×10^{-5}	(2.37,0.19) 8.53×10^{-6}
10	(1.93,0.26) 3.35×10^{-7}	(2.24,0.22) 6.86×10^{-8}	(2.33,0.19) 3.91×10^{-8}	(2.39,0.18) 3.36×10^{-8}

Table 4.5: Optimum 2-ary (w, q) MCPCM Signalling Scheme with Error Probability Upper Bounds

The optimum 2-ary MCPCM system, optimum for $5T$ observation, with signal parameters ($w = 2.37$ and $q = 0.19$), outperforms PSK by nearly 1.6 dB. In the previous section, we have seen that the limiting SNR gain for 2-ary MCPCM system is 1.66 dB. From these two observations, it is apparent that nearly all the potential of 2-ary MCPCM can used by employing the optimum 5-bit MCPCM receiver. However, the complexity of this receiver is quite high. Furthermore, it is noted that an improvement of about 0.75 dB is possible in going from $3T$ to $5T$ observation and about 0.25 dB in going from $3T$ to $5T$ observation. These observations may be used to strike a compromise between the complexity and energy performances of the receiver. Comparing the performance of 2-ary MCPCM system with that of the well-known 2-ary CPFSK system, we observe that the former has nearly 0.5 dB advantage over the latter.

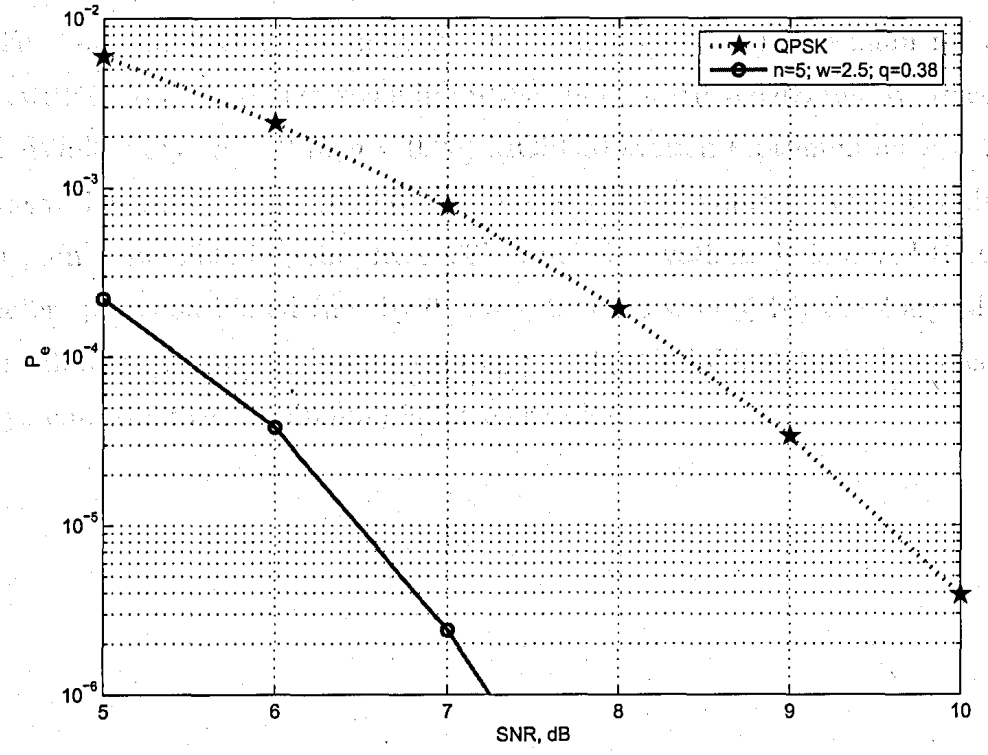

Figure 4.5: Optimum Error Probability Performance of 4-ary Chirp ($w = 2.5, q = 0.38$) and $n = 5$ with QPSK Modulation

SNR \ n	2	3	4	5
6	(2.73,0.25) 2.69×10^{-4}	(2.43,0.40) 6.78×10^{-5}	(2.48,0.39) 3.27×10^{-5}	(2.49,0.38) 2.38×10^{-5}
8	(2.75,0.25) 2.26×10^{-6}	(2.48,0.40) 2.00×10^{-7}	(2.51,0.39) 1.00×10^{-7}	(2.50,0.38) 7.15×10^{-8}
10	(2.76,0.25) 1.69×10^{-9}	(2.51,0.40) 3.06×10^{-11}	(2.52,0.38) 1.68×10^{-11}	(2.51,0.38) 3.36×10^{-11}

Table 4.6: Optimum 4-ary (w, q) MCPCM Signalling Scheme with Error Probability Upper Bounds

For 4-ary MCPCM, the optimum $(w = 2.5, q = 0.38)$ (optimum for $n = 5$) system with $5T$ observation gives an improvement of nearly 3.6 dB relative to coherent QPSK. While 4-ary $(w = 2.75, q = 0.25)$ MCPCM system (optimum for $n = 2$) with $2T$ observation provides nearly 2.6 dB gain relative to coherent QPSK, only 1 dB further gain is possible in going from $2T$ to $5T$ observation. It is noted that in the parameter space considered (i.e. by $0 < q \leq 2$ and $0 < w \leq 10$) the 4-ary MCPMC system exhibits only an improvement of up to 3.44 dB Table 4.3 relative to coherent PSK system, using the minimum distance criterion.

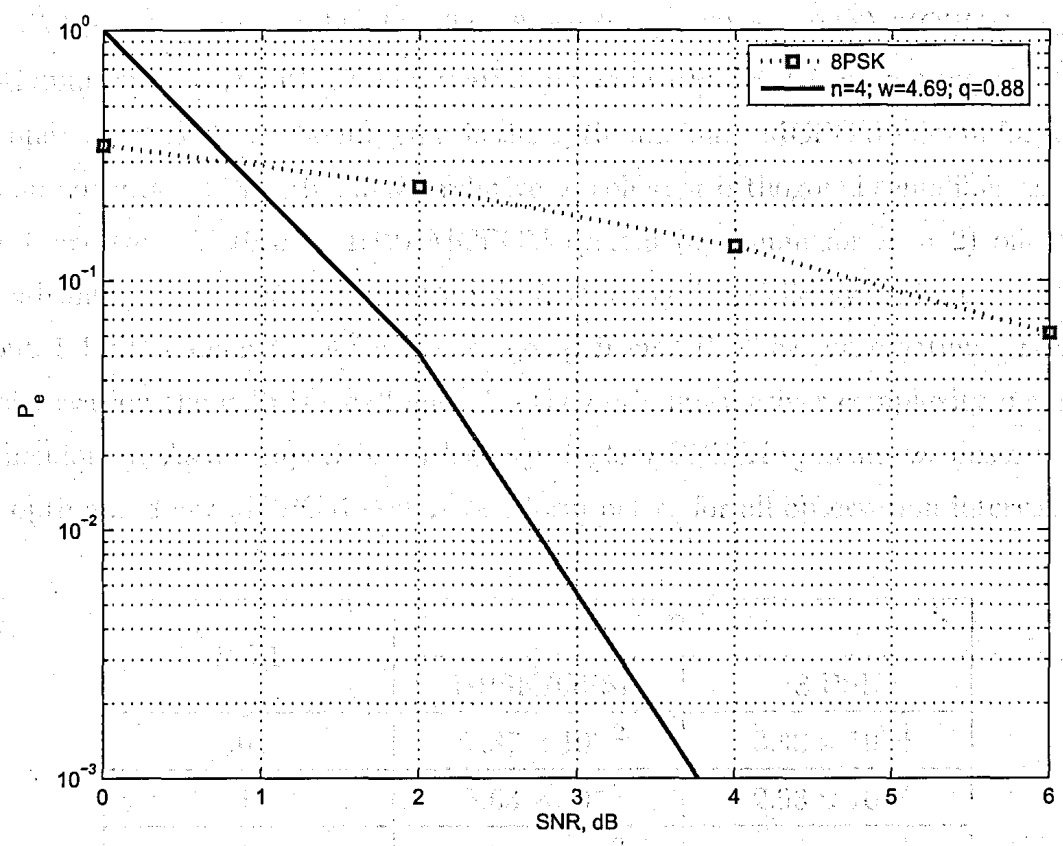

Figure 4.6: Optimum Error Probability Performance of 8-ary Chirp $(w = 4.69, q = 0.88)$ and $n = 4$ with 8-PSK Modulation

SNR \ n	2	3	4
6	(4.10,1.12) 6.23×10^{-5}	(4.71,0.88) 9.39×10^{-6}	(4.71,0.88) 4.37×10^{-6}
8	(4.10,1.12) 1.22×10^{-7}	(4.69,0.88) 7.99×10^{-9}	(4.69,0.88) 3.36×10^{-9}
10	(4.10,1.12) 9.04×10^{-11}	(4.68,0.88) 1.88×10^{-13}	(4.68,0.88) 6.83×10^{-14}

Table 4.7: Optimum 8-ary (w, q) MCPCM Signalling Scheme with Error Probability Upper Bounds

With reference to table 4.8. The 8-ary ($w = 4.69, q = 0.88$) MCPCM system (optimum for $n = 4$) with $4T$ observation offers nearly 7.8 dB improvement relative to coherent octal PSK system. That is the optimum 8-ary MCPCM system for $n = 4$ has an advantage of nearly 2.9 dB relative to coherent orthogonal signalling scheme. The 8-ary ($w = 4.10, q = 1.12$) MCPCM system (optimum for $n = 2$) offers 1.8 dB advantage over coherent octal PSK. With 8-ary MCPCM system, there is only about 1.4 dB gain in performance in going from $2T$ to $5T$ observation. Beyond $5T$observation the gain is small and also the optimum receiver complexity increases tremendously. As a comparison with 8-ary single-h CPFSK systems, we observe that the optimum 8-ary MCPCM systems perform better for all observation intervals.

SNR	P_e	
	BPSK/QPSK	8-PSK
0	7.87×10^{-2}	3.48×10^{-1}
1	5.63×10^{-2}	2.93×10^{-1}
2	3.75×10^{-2}	2.38×10^{-1}
3	2.29×10^{-2}	1.85×10^{-1}
4	1.25×10^{-2}	1.37×10^{-1}
5	5.95×10^{-3}	9.55×10^{-2}
6	2.39×10^{-3}	6.14×10^{-2}
7	7.73×10^{-4}	3.59×10^{-2}
8	1.91×10^{-4}	1.85×10^{-2}
9	3.36×10^{-5}	8.24×10^{-3}
10	3.87×10^{-6}	3.03×10^{-3}

Table 4.8: Probability of Error for 2,4 and 8-PSK

4.6 Summary

In this Chapter we have examined MCPCM signals for M-ary data transmission. A general description of an MCPCM system is given and the independent modulation parameters that characterize such a system are identified and described. The optimum and suboptimum receiver structures for coherent detection for arbitrary observation intervals are derived and their performances in terms of symbol error rates are estimated. Also, using the notion of minimum Euclidean distance in signal-space, the achievable SNR gain possible with MCPCM system relative to PSK systems are established. The results reveal that the concept of continuous phase can be successfully applied to digital transmission using chirp signals.

The symbol error probability upper bound on the performance of the optimum coherent MCPCM receiver is a function of signal modulation parameters,(w, q), the receiver decision observation length, number of levels of data, and the received signal-to-noise ratio. Minimization of symbol error probability for MCPCM systems can only be solved numerically. Employing this approach, optimum 2-, 4-, and 8-ary MCPCM systems have been determined as a function of decision observation length and received SNR. It is borne by our results that the optimum MCPCM modulation parameters is a mild function of the received SNR and as well as a function of observation interval.

It is shown that the 2-ary MCPCM system, for $5T$ observation, offers nearly 1.6 dB improvement in performance relative to coherent PSK, 4-ary MCPCM system has nearly 3.6 dB gain over QPSK, and 8-ary MCPCM system over 5T observation length offers nearly 8 dB improvement relative to octal PSK. Also, it is shown that the 2-, 4-, and 8-ary MCPCM systems have limiting SNR gains relative to coherent PSK systems of 1.66, 4.67, and 6.43 dB, respectively.

Although, the results of this Chapter provide performance estimates that are inherent in MCPCM systems, for successful application further examination of bandwidth occupancy, receiver complexity, synchronization techniques etc. associated with MCPCM systems are required.

Chapter 5
Non-Coherent Detection of MCPCM Signals in Gaussian Noise

5.1 Introduction

In this chapter, we extend the results of the previous chapter to cover the case of non-coherent reception of MCPCM signals. An apparent advantage of non-coherent system is that they do not require carrier tracking, which in fact is mandatory in coherent systems. The primary objective of this chapter is to assess the performance ability of non-coherent MCPCM signals in AWGN channel. The optimum non-coherent MCPCM receiver is derived and by minimization of upper bound on its performance, optimum non-coherent MCPCM signalling schemes are determined.

5.2 Structure of Optimal MCPCM Non-Coherent Receiver

The received MCPCM signal buried in AWGN with one-sided power spectral density of N_0 $watts/Hz$ can be written as:

$$r(t) = S(t, a_\delta, A_k, \theta), \quad 0 \leq t \leq nT \tag{5.1}$$

where nT is the observation length, θ is the random phase uniformly distributed in $(0, 2\pi)$. The detection strategy is to observe $r(t)$ and produce an estimate $\hat{a}$ of the symbol a_δ transmitted during the decision symbol interval. The detection problem

clearly is a composite hypothesis testing problem [2]. for which the solution is likelihood ratio test. The likelihood parameters computed by the optimal receiver are given by:

$$\begin{aligned}
\Lambda_1 &= \int_\theta \sum_{k=1}^{m} \exp\left[\frac{2}{N_0}\int_0^{nT} r(t)S(t, a_\delta = +1, A_k, \theta)dt\right] P_\theta(\theta)d\theta \\
&\vdots \\
\Lambda_M &= \int_\theta \sum_{k=1}^{m} \exp\left[\frac{2}{N_0}\int_0^{nT} r(t)S(t, a_\delta = -(m-1), A_k, \theta)dt\right] P_\theta(\theta)d\theta
\end{aligned} \tag{5.2}$$

upon performing integrations over θ in (5.2), the likelihood parameters become:

$$\Lambda_j = \sum_{k=1}^{m} I_0\left(\frac{2}{N_0}x_{jk}\right), \quad j = 1, 2, \ldots, M \tag{5.3}$$

where

$$x_{jk}^2 = I_{jk}^2 + Q_{jk}^2 \tag{5.4}$$

with

$$I_{jk} = \begin{cases} \int_0^{nT} r(t)S(t, a_\delta = +j, A_k, 0)dt, & j \ \ odd \\ \int_0^{nT} r(t)S(t, a_\delta = -(j-1), A_k, 0)dt, & j \ \ even \end{cases} \tag{5.5}$$

and

$$Q_{jk} = \begin{cases} \int_0^{nT} r(t)S(t, a_\delta = +j, A_k, \frac{\pi}{2})\ dt, & j \ \ odd \\ \int_0^{nT} r(t)S(t, a_\delta = -(j-1), A_k, \frac{\pi}{2})\ dt, & j \ \ even \end{cases} \tag{5.6}$$

The structure of the optimum receiver implied by (5.3) is shown in Fig. 5.1. This receiver essentially computes M likelihood parameters and produce a decision by

choosing the largest of these M parameters.

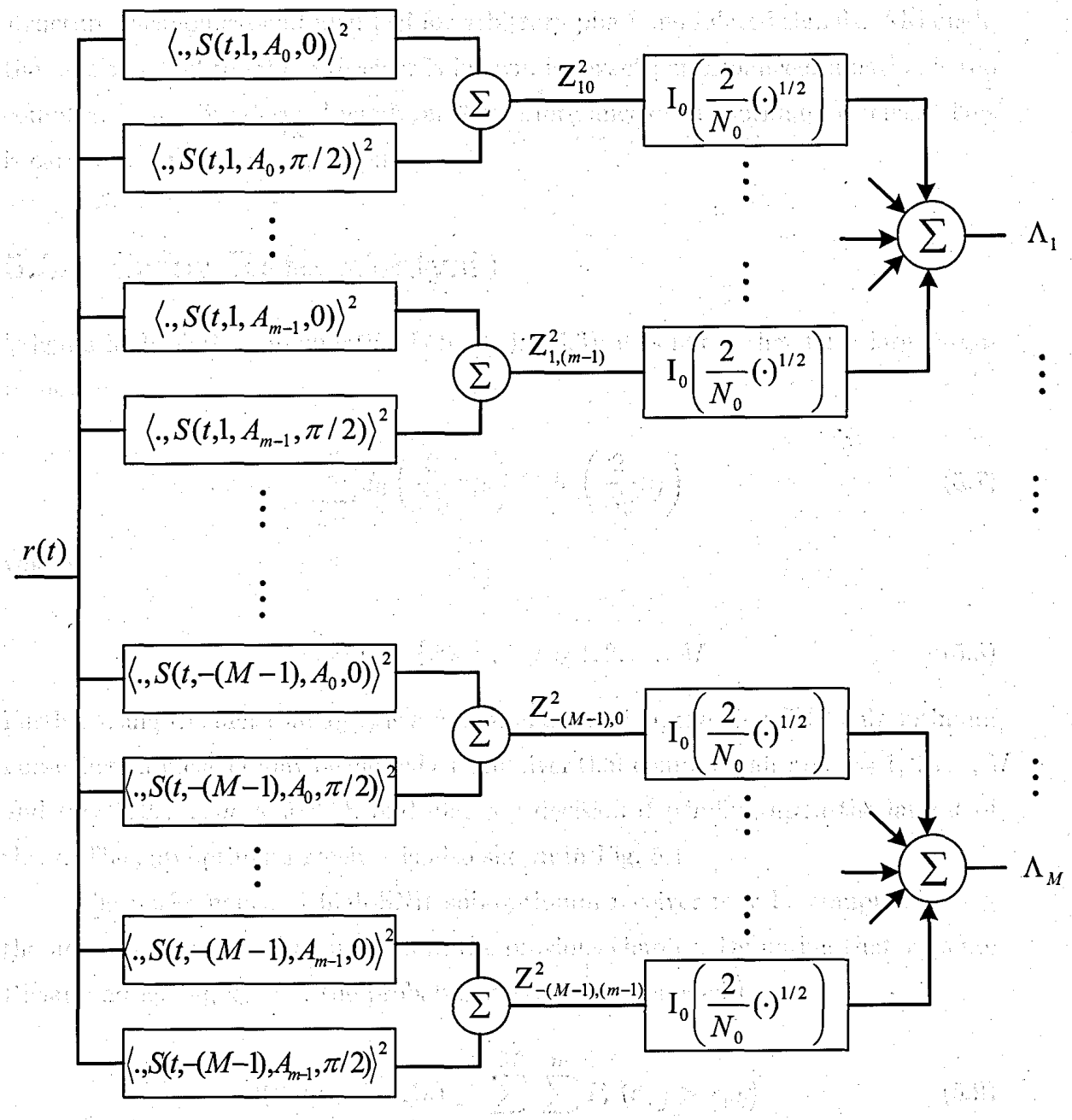

Figure 5.1: Optimum Non-Coherent Receiver Structure

$$\left(\langle x(t), y(t)\rangle^2 \triangleq \left[\int_0^{nT} x(t)y(t)dt\right]^2\right)$$

If jth of the M parameters is the largest, the receiver decides $a_\delta = +j$ or $a_\delta = -(j-1)$ accordingly as whether j is odd or even. It is noted that the optimum receiver structure is canonical and identical for arbitrary phase modulated signals. Although, the precise structure of the receiver is known, its exact performance evaluation is too complex. Hence, we derive bounds on the performance of the optimum receiver. This is carried out in the next section.

5.3 Error Rate Analysis

When a high-SNR approximation is made in (5.3), it is noted that for a large arguments:

$$\sum_{k=1}^{m} I_0\left(\frac{2}{N_0}x_{jk}\right) \cong I_0\left(\frac{2}{N_0}\tilde{x_j}\right) \tag{5.7}$$

where

$$\tilde{x_j} = \max_k \{x_{jk}\}, \quad j = 1, 2, \ldots, M \tag{5.8}$$

Further using the fact that $I_0(.)$ is a monotonic function, the high-SNR sub-optimum non-coherent receiver may be viewed as a receiver that computes all $x_{jk}, j = 1, 2, \ldots, M$ and $k = 1, 2, \ldots, m = M^{n-1}$, and makes a decision depending upon the largest of these. The sub-optimum receiver is also shown in Fig. 5.1

The performance of high-SNR sub-optimum receiver may be computed using the union bounding technique used in the previous chapter. By noting that x_{jk}s are Rician and letting $a_\delta = u$, the probability of error is bounded by:

$$P(\in / a_\delta = u, A_k) \leq \sum_{\substack{v=1 \\ v \neq a_\delta}}^{M} \sum_{j=1}^{m} P_r\left(x_{vj} > x_{uk}\right) \tag{5.9}$$

Averaging over all possible data symbols in the decision symbol interval and over all possible data sequences A_k, the probability of an error is given by:

$$P(\in) \leq \frac{1}{M}\frac{1}{m}\sum_{u=1}^{M}\sum_{\substack{v=1 \\ v\neq u}}^{M}\sum_{j=1}^{m}\sum_{k=1}^{m} P_r\left(x_{vj} > x_{uk}\right) \tag{5.10}$$

The problem now is to obtain an expression for the probability of Rician variable exceeding another, which is given by:

$$P_r\left(x_{vj} > x_{uk}\right) = \frac{1}{2}\left(1 - Q(\sqrt{b}, \sqrt{a}) + Q(\sqrt{a}, \sqrt{b})\right) \tag{5.11}$$

where

$$\left\{ \begin{array}{c} a \\ \\ b \end{array} \right\} = \frac{nE}{2N_0}\left[1 \mp \sqrt{1 - |\rho_c(v_j, u_k)|^2}\right] \tag{5.12}$$

and $\rho_c(v_j, u_k)$ is the normalized complex correlation between the complex envelopes $S_c(t, a_\delta = v, A_j)$ and $S_c(t, a_\delta = u, A_k)$, and these are given by:

$$S_c(t, a_\delta = v, A_k) = \sqrt{\frac{2E}{T}} \exp\left[j\phi(t, a_\delta = v, A_k)\right] \tag{5.13}$$

Using (5.13) and noting that the data sequences $(a_\delta = v, A_j)$ and $(a_\delta = u, A_k)$ are $a_1^j, a_2^j, \ldots, a_\delta = v, \ldots, a_n^j$ and $a_1^k, a_2^k, \ldots, a_\delta = u, \ldots, a_n^k$ a closed form expression for $\rho_c(v_j, u_k)$ can be obtained. The number of computations in the evaluation of (5.10) can be significantly reduced by recognizing and identifying redundant different sequences. It can be shown that an expression equivalent to (5.10) can be shown to be given by:

$$P(\in) < (M-1)\, M^{n-1} \int_{\tilde{\gamma}} \frac{1}{2}\left[1 - Q(\sqrt{b}, \sqrt{a}) + Q(\sqrt{a}, \sqrt{b})\right] p(\tilde{\gamma})\, d\gamma \tag{5.14}$$

where $\int_{\tilde{\gamma}} d\tilde{\gamma}$ and $p(\tilde{\gamma})$ are as given in (4.30) and (4.31), respectively. In the next section, we present the error probability performance of MCPCM systems.

5.4 Numerical Results and Discussion

The symbol error probability upper bound on the performance of the optimum non-coherent MCPCM receiver can be computed using (5.14). As in the coherent case, the error probability is a function of : i) n , observation length; ii) E_b/N_0 , Signal-to-Noise Ratio; iii) M , size of input data alphabet; and iv) (w, q) , set of modulation parameters. Further, in the case of non-coherent case, the error probability is a function of the location of the decision data symbol, δ . The set of signal modulation parameters (w, q) that should be chosen is obviously the one that minimizes the symbol error probability upper bound of (5.14). The minimization problem cannot be tackled analytically and, therefore, numerical technique is in order. Using this technique, at SNRs of 6, 8, and 10 dB, sets (w, q) that minimize (5.14) have been determined for $2 \leq n \leq 5, M = 2, 4, 8$ and $1 \leq \delta \leq n$. The results are tabulated in Tables 5.1 to 5.8.

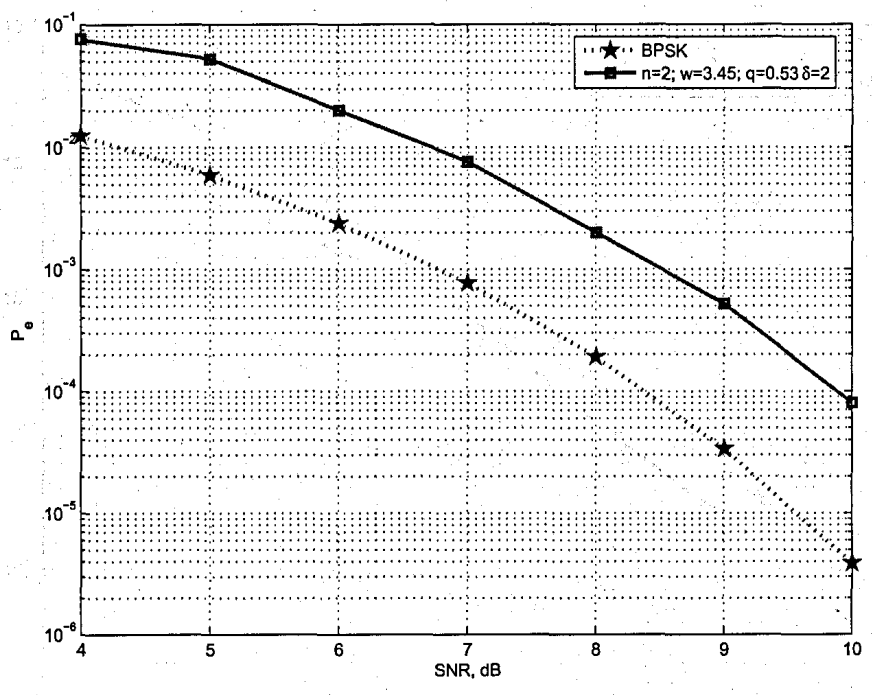

Figure 5.2: Error Probability Performance of 2-ary non-coherent MCPCM $(w = 3.45, q = 0.53)$, $\delta = 2$ and $n = 2$ with BPSK Modulation

As an example, the performance of non-coherent MCPCM is plotted with an observation length of $n = 2$ and $n = 4$ in Fig. 5.2 and Fig.5.3, respectively. When the performance of non-coherent MCPCM is compared with coherent MPSK systems, it becomes apparent that non-coherent 2-ary MCPCM system can outperform coherent BPSK. For example, the optimum non-coherent 2-ary MCPCM receiver with an observation length of 4 bit intervals and the decision on the second bit data can outperform BPSK. This superiority is achieved for $E_b/N_0 > 7\ dB$ (i.e. for error rates less than 10^{-3}). An overall gain of about 1 dB is inherent in non-coherent binary MCPCM system relative to BPSK. The optimum non-coherent $(w = 2.60, q = 0.26)$ MCPCM system with 5 symbol observation length and decision on the middle bit yields 4.3 dB SNR gain over non-coherent orthogonal system.

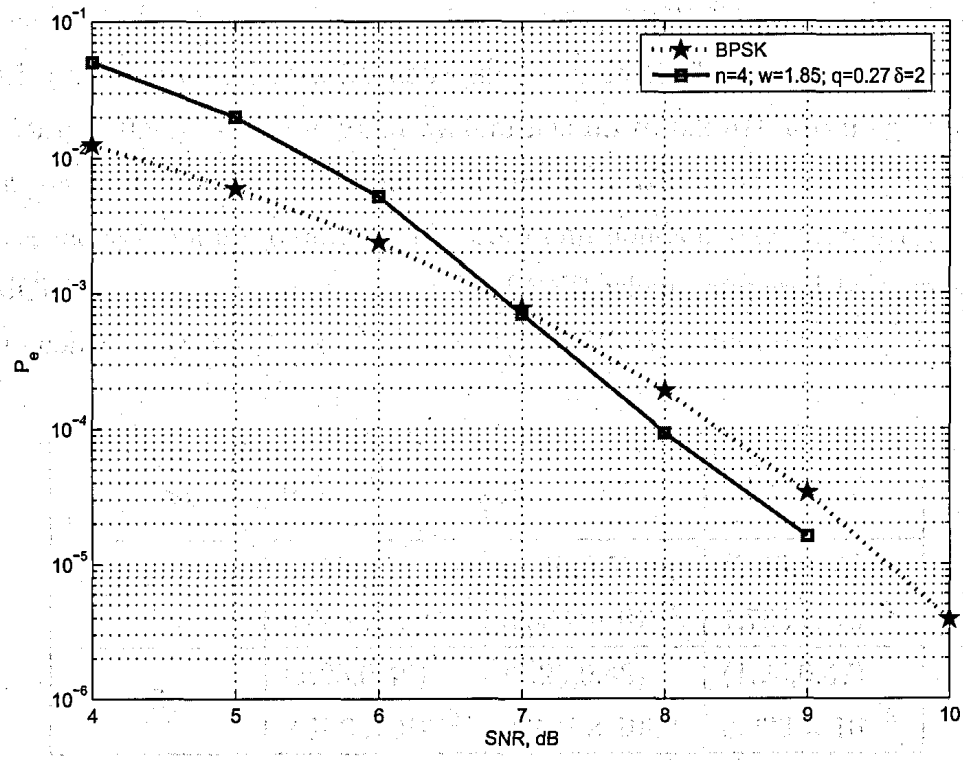

Figure 5.3: Error Probability Performance of non-coherent MCPCM with $(w = 1.85, q = 0.27)$, $\delta = 2$ and $n = 4$

It is noted that the upper bound error rate performance of the optimum non-coherent MCPCM receiver is a function of δ , the location of the decision data symbol. From Tables 5.1 to 5.8, it is observed that optimum decision symbol location is given by $\delta = int\left(\frac{n}{2}\right) + 1$ for n odd and $\delta = \left(\frac{n}{2}\right)$ or $\left(\frac{n}{2} + 1\right)$ for n even. Also, we note that this behaviour of the optimum decision symbol location,δ , is independent of the received SNR.

The 4-ary non-coherent $(w = 0.55, q = 0.84)$ MCPCM modulation (optimum for $n = 2$ and $\delta = 2$) with $5T$ observation performs nearly as well as coherent QPSK for error rates less than 10^{-4} and outperforms QPSK marginally for error rates less than 10^{-5} (i.e. for E_b/N_0 >10 dB). The optimum 4-ary non-coherent $(w = 4.65, q = 0.76)$ MCPCM system, for $4T$ observation length with decision on the second symbol, is inferior to the corresponding optimum 4-ary coherent MCPCM system by nearly 1.6 dB.

The symbol error rates for non-coherent 8-ary MCPCM system have been compared with symbol error rates for coherent 8-ary PSK. The optimum non-coherent $(w = 4.70, q = 0.88)$ 8-ary MCPCM system has up to 6.2 dB advantage relative to coherent 8-ary PSK. However, in the former case $3T$ observation length and decision on the second symbol are required. The optimum non-coherent $(w = 4.70, q = 0.88)$ 8-ary MCPCM system is worse in terms of SNR when compared to corresponding optimum coherent $(w = 4.69, q = 0.88)$ 8-ary MCPCM system by nearly 1.4 dB.

SNR, dB / δ	6	8	10
1	(3.45,0.53) 2.468×10^{-2}	(3.45,0.53) 3.333×10^{-3}	(3.45,0.53) 1.705×10^{-4}
2	(1.25,0.48) 2.106×10^{-2}	(1.25,0.48) 2.370×10^{-3}	(1.25,0.47) 8.233×10^{-5}

Table 5.1: Optimum (w, q) 2-ary MCPCM Systems with Error Probability Upper Bounds (n=2)

SNR, dB / δ	6	8	10
1	(3.85,0.78) 1.810×10^{-2}	(3.85,0.76) 2.194×10^{-3}	(3.75,0.71) 1.151×10^{-4}
2	(3.45,0.50) 1.033×10^{-2}	(3.50,0.50) 6.797×10^{-4}	(3.45,0.50) 1.196×10^{-5}
3	(1.70,0.31) 1.539×10^{-2}	(1.65,0.33) 1.418×10^{-3}	(1.60,0.35) 4.379×10^{-5}

Table 5.2: Optimum (w, q) 2-ary MCPCM Systems with Error Probability Upper Bounds (n=3)

SNR, dB / δ	6	8	10
4	(2.00,0.21) 1.144×10^{-2}	(1.85,0.27) 1.036×10^{-3}	(1.75,0.31) 3.552×10^{-5}
2	(3.914,0.72) 6.914×10^{-3}	(3.85,0.69) 3.180×10^{-4}	(3.90,0.71) 3.343×10^{-6}
3	(0.5,0.69) 6.914×10^{-3}	(0.5,0.69) 3.183×10^{-4}	(0.50,0.70) 3.386×10^{-6}
1	(4.00,0.85) 1.487×10^{-2}	(3.90,0.79) 1.883×10^{-3}	(3.75,0.71) 1.052×10^{-5}

Table 5.3: Optimum (w, q) 2-ary MCPCM Systems with Error Probability Upper Bounds (n=4)

SNR, dB / δ	6	8	10
3	(2.70,0.28) 4.110×10^{-3}	(2.60,0.26) 1.286×10^{-4}	(2.65,0.26) 8.010×10^{-7}

Table 5.4: Optimum (w, q) 2-ary MCPCM Systems with Error Probability Upper Bounds (n=5)

SNR, dB / δ	6	8	10
2	(0.55,0.84) 1.045×10^{-2}	(0.55,0.84) 4.974×10^{-4}	(0.55,0.84) 5.837×10^{-6}
1	(3.65,0.24) 1.135×10^{-2}	(4.80,0.86) 5.566×10^{-4}	(4.80,0.85) 6.596×10^{-6}

Table 5.5: Optimum (w, q) 4-ary MCPCM Systems with Error Probability Upper Bounds (n=2)

SNR, dB / δ	6	8	10
3	(4.80,0.76) 2.770×10^{-3}	(4.90,0.76) 3.525×10^{-5}	(4.90,0.76) 5.647×10^{-8}

Table 5.6: Optimum (w, q) 4-ary MCPCM Systems with Error Probability Upper Bounds (n=3)

SNR, dB / δ	6	8	10
2	(4.65,0.76) 1.686×10^{-3}	(4.65,0.76) 1.191×10^{-5}	(4.65,0.75) 7.371×10^{-9}

Table 5.7: Optimum (w, q) 4-ary MCPCM Systems with Error Probability Upper Bounds (n=4)

n	δ	SNR, dB
		8 dB
2	2	$\{0.40, 0.42\}$
3	2	$\{4.70, 0.88\}$

Table 5.8: Optimum (w, q) 8-ary MCPCM Systems with Error Probability Upper Bounds

5.5 Summary

In this Chapter the optimum non-coherent MCPCM receiver is derived and the symbol error rate of this receiver is found using high-SNR union upper bound. Explicit expressions for determining this upper bound have been obtained. The parameters that influence the performance of the non-coherent receiver have been identified and optimum MCPCM systems that minimize the symbol error rates have been found as a function of observation length, decision symbol location and receiver SNR.

It is shown that 2-, 4-, and 8-ary non-coherent MCPCM systems can outperform BPSK, QPSK, and 8-ary PSK systems. However, the receiver complexities associated with MCPCM systems are much higher compared to MPSK systems.

Chapter 6
Concluding Remarks and Suggestions for Future Work

6.1 Introduction

In this Chapter, we summarise the contributions of this thesis and the conclusions from the results obtained. Also, we outline areas for further research in the light of the needs of modern wireless communication systems. In particular, we discuss the possible future applications for M-ary chirp modulations. In Section 6.2, summary of contributions to the thesis is given and in Section 6.3, suggestions for further research work are outlined.

6.2 Summary of Contributions

In this thesis we have proposed M-chirp modulations for data transmission. These wide-band modulations have inherent interference rejection capability of spread-spectrum type of systems. Furthermore, chirp modulations are particularly attractive in applications where immunity against Doppler shift and fading due to multipath propagation is important.

In Chapter 2, a general description of the signalling technique using chirp modulation for M-ary data transmission is given. The parameters that describe the modulation parameters explained and illustrated. These parameters are: h, modulation index, and w , frequency sweep width. Since these two are related by the relationship $q = h - w$, we have chosen to represent a specific chirp modulation system using the set of modulation parameters (q, w) . Two classes of chirp modulations are considered: i) M-ary (q, w) chirp modulation without memory (or discontinuous phase

chirp modulation); and ii) M-ary (q, w) chirp modulation with memory referred to as (q, w) M-ary Continuous Phase Chirp Modulation (MCPCM).

The problems of coherent and non-coherent detection of M-ary chirp modulated signal in AWGN channel are considered in Chapter 3. Using detection theory we have derived the structures of optimum coherent and non-coherent receivers. Closed-form expressions for estimating the symbol error rate performances of these receivers have been derived. Optimum coherent and non-coherent M-ary (q, w) chirp systems have been determined, using exhaustive numerical search that minimize the probability of symbol error. It is shown that optimum coherent 2-ary $(w = 1.85, q = 0.28)$ can provide an SNR advantage of nearly 2 dB relative to well-known 2-ary Orthogonal FSK system. It is observed that optimum coherent 4-ary $(w = 2.4, q = 0.4)$ chirp modulation is marginally superior to 4-ary Orthogonal FSK and is only inferior to QPSK by nearly 2 dB . The optimum coherent 8-ary $(w = 0.25, q = 0.95)$ chirp system performs nearly as good as 8-ary PSK system. An investigation of the sensitivity symbol error rates to variation in modulation parameters w and q is also given. As regards non-coherent M-ary (w, q) chirp modulation we note that it equivalent to M-ary non-coherent Orthogonal FSK. A wide range of can be found that meet this criterion. It is noted that using M-ary chirp modulation, in general, one can strike trade-offs between symbol error rate and bandwidth of the signal though appropriate choice of modulation parameters.

While in Chapter 3 we considered memory-less M-ary chirp modulated signals, in Chapters 4 and 5, by introducing memory into these signals we have examined a class of signals referred to as MCPCM. Memory in these signals has been introduced by constraining the phase of the signal to be continuous at bit transitions. One of the advantages of introducing memory is that symbol error rate performance can be improved by observing the received signal over intervals longer than one symbol interval. In Chapter 4 we have considered coherent multiple symbol detection MCPCM signals in AWGN channel and the corresponding non-coherent case is addressed in Chapter 5. The structures of optimum coherent and non-coherent receivers have been derived using composite hypothesis testing theory. The receiver structures are non-linear and complex. Since it is too difficult to evaluate precise symbol error rates of

these receivers, we have established error rate bounds at high values of SNR. Again, a thorough investigation has been carried out to arrive at optimum M-ary (w, q) Chirp systems, both coherent as well as non-coherent, through numerical minimization of symbol error rate bounds. Also, in Chapter 4, we have established upper bounds on the minimum distance squared for MCPCM. These bounds can be used to understand the ultimate ability of MCPCM to operate over AWGN channel and also provide a means of comparison with other modulations of which the distance properties are known. Below we list out the chief results from Chapters 4 and 5.

- Coherent 2-ary MCPCM system has up to 1.66 dB (limiting) SNR advantage relative to Binary PSK. 2-ary MCPCM systems exist, which in conjunction with 5-symbol optimum coherent receiver provides nearly all the performance potential inherent in 2-ary MCPCM

- Coherent 4-ary MCPCM has up to 4.7 dB (limiting) SNR gain relative to QPSK. However, with an optimum coherent receiver of 5-symbol observation length, only about 3.5 dB SNR relative to QPSK can be achieved

- Coherent 8-ary MCPCM system has a limiting advantage of 6.4 dB relative to corresponding PSK and has 2.9 dB SNR advantage over corresponding orthogonal signalling scheme

- Non-coherent 2-ary MCPCM systems exist that in conjunction with the corresponding optimum receiver outperforms coherent 2-ary PSK. However, to achieve this superiority the observation length of the receiver must be at least 4 symbol intervals

- Non-coherent 4-ary MCPCM system has up to 1.9 dB advantage over coherent QPSK

- Non-coherent 8-ary MCPCM system has the ability to outperform coherent 8-ary FSK by nearly 1.3 dB . A 4-symbol optimum non-coherent receiver is required to achieve this superiority

- Optimum non-coherent MCPCM receivers provide best performances when perform decisions on the middle bit (s) for any arbitrary number of observation intervals

6.3 Suggestions for Future Work

In any communication system the transmitted signals are subject to various interferences besides the usual additive channel considered in this thesis. A direct extension of the results of thesis is to assess the ability of M-ary chirp modulated signals in additive white Gaussian noise and multi-path fading channels.

A combination of M-ary chirp modulation and pseudorandom coding can be designed for application in a multiple user environment. In a multi-user environment, co-channel interference and adjacent channel interferences are major sources of performance degradation. It would be interesting to design and analyse multi-user access communication systems using chirp modulation.

References

[1] A. Goldsmith, *Wireless Communications.* Cambridge University Press, 2005.

[2] J. G. Proakis, *Digital communications, 4th ed.* McGraw-Hill, 2001.

[3] R. C. Dixon, *Spread spectrum systems.* Wiley, 1976.

[4] L. M. DAO, "WIRELESS COMMUNICATIONS USING CHIRP SIGNALS," 2008.

[5] M. Huemer, A. Koppler, C. Ruppel, L. Reindl, A. Springer, and R. Weigel, "Saw based chirp fourier transform for ofdm systems," in *Ultrasonics Symposium, 1999. Proceedings. 1999 IEEE*, vol. 1, 1999, pp. 373 –376 vol.1.

[6] [Online]. Available: http://www.ieee802.org/15/pub/TG4a.html

[7] [Online]. Available: http://www.nanotron.com/EN/PR_nN_TRX.php

[8] C. Cook, "Linear fm signal formats for beacon and communication systems," *Aerospace and Electronic Systems, IEEE Transactions on*, vol. AES-10, no. 4, pp. 471 –478, july 1974.

[9] M. R. Winkler, "Chirp signals for communications," in *Western Electronic Show and Convention*, August 1962.

[10] A. Berni and W. Gregg, "On the utility of chirp modulation for digital signaling," *Communications, IEEE Transactions on*, vol. 21, no. 6, pp. 748 – 751, jun 1973.

[11] G. Gott and J. Newsome, "H.f. data transmission using chirp signals," *Electrical Engineers, Proceedings of the Institution of*, vol. 118, no. 9, pp. 1162 –1166, september 1971.

[12] D. Dayton, "Fm "chirp" communications: Multiple access to dispersive channels," *Electromagnetic Compatibility, IEEE Transactions on*, vol. EMC-10, no. 2, pp. 296 –297, june 1968.

[13] G. Gott and A. Karia, "Differential phase-shift keying applied to chirp data signals," *Electrical Engineers, Proceedings of the Institution of*, vol. 121, no. 9, pp. 923 –928, september 1974.

[14] M. Kowatsch, F. Seifert, and J. Lafferl, "Comments on transmission system using pseudonoise modulation of linear chirps," *Aerospace and Electronic Systems, IEEE Transactions on*, vol. AES-17, no. 2, pp. 300 –303, march 1981.

[15] S. El-Khamy and S. Shaaban, "Matched chirp modulation: detection and performance in dispersive communication channels," *Communications, IEEE Transactions on*, vol. 36, no. 4, pp. 506 –509, apr 1988.

[16] A. Elhakeem and A. Targi, "Performance of hybrid chirp/ds signals under doppler and pulsed jamming," in *Global Telecommunications Conference, 1989, and Exhibition. Communications Technology for the 1990s and Beyond. GLOBECOM '89., IEEE*, nov 1989, pp. 1618 –1623 vol.3.

[17] M. Kowatsch and J. Lafferl, "A spread-spectrum concept combining chirp modulation and pseudonoise coding," *Communications, IEEE Transactions on*, vol. 31, no. 10, pp. 1133 – 1142, oct 1983.

[18] X. Wang, M. Fei, and X. Li, "Performance of chirp spread spectrum in wireless communication systems," in *Communication Systems, 2008. ICCS 2008. 11th IEEE Singapore International Conference on*, nov. 2008, pp. 466 –469.

[19] W. Hirt and S. Pasupathy, "Continuous phase chirp (cpc) signals for binary data communication-part i: Coherent detection," *Communications, IEEE Transactions on*, vol. 29, no. 6, pp. 836 – 847, jun 1981.

[20] ——, "Continuous phase chirp (cpc) signals for binary data communication–part ii: Noncoherent detection," *Communications, IEEE Transactions on*, vol. 29, no. 6, pp. 848 – 858, jun 1981.

[21] K. Raveendra, "Digital transmission using multimode phase-continuous chirp signals," *Communications, IEE Proceedings-*, vol. 143, no. 2, p. 87, apr 1996.

[22] B. A. Dave and R. K. Rao, "Data transmission using digital asymmetric phase continuous chirp signals," *World Wireless Congress, Palo Alto*, vol. 24-27, pp. 383–388, May 2005.

[23] A. Hengstler, "A novel chirp modulation spread spectrum technique for multiple access," 2001.

[24] A. Springer, W. Gugler, M. Huemer, R. Koller, and R. Weigel, "A wireless spread-spectrum communication system using saw chirped delay lines," *Microwave Theory and Techniques, IEEE Transactions on*, vol. 49, no. 4, pp. 754 –760, apr 2001.

[25] H. Shen, S. Machineni, C. Gupta, and A. Papandreou-Suppappola, "Time-varying multichirp rate modulation for multiple access systems," *Signal Processing Letters, IEEE*, vol. 11, no. 5, pp. 497 – 500, may 2004.

[26] H. Liu, "Multicode ultra-wideband scheme using chirp waveforms," *Selected Areas in Communications, IEEE Journal on*, vol. 24, no. 4, pp. 885 – 891, april 2006.

[27] M. Fanyu and G. Xuemai, "A combined chirp signal modulation technique for multiple access system," *Information Technology Journal 10(2)*, pp. 416–422, 2011.

[28] R. K. R. A. Kadri and J. Jiang, "Low-power chirp spread spectrum signals for wireless communications within nuclear power plants," *ANS, Nuclear Technology*, vol. 166, no. 2, pp. 156–169, May 2009.

[29] A. Kadri, "Low-Power Chirp Signal For Wireless Data Communication in Industrial Environments," Ph.D. dissertation, University of Western Ontario, 2009.

[30] T. H. Van, *Detection, estimation, and modulation theory.* Wiley, 2001.

Appendix A
Normalized Correlation for M-ary Chirp Signals

The normalized correlation for M-ary chirp signals is derived here. Assume the the transmitted signal represents data symbol d_j and the received signal represents data symbol d_i. These signals are given by:

$$\begin{aligned} S(t,d_j) &= \sqrt{\frac{2E_s}{T}}\ \cos\left[w_c t + d_j \pi \left\{h\left(\tfrac{t}{T}\right) - w\left(\tfrac{t}{T}\right)^2\right\}\right] \\ S(t,d_i) &= \sqrt{\frac{2E_s}{T}}\ \cos\left[w_c t + d_i \pi \left\{h\left(\tfrac{t}{T}\right) - w\left(\tfrac{t}{T}\right)^2\right\}\right] \end{aligned} \tag{A.1}$$

The normalized cross correlation between these signals is defined by:

$$\rho(j,i) = \frac{1}{E_s}\int_0^T S(t,d_j)\ S(t,d_i)dt \tag{A.2}$$

Substitute (A.1) in (A.2)

$$\begin{aligned} \rho(j,i) = \frac{1}{E_s}\int_0^T &\sqrt{\frac{2E_s}{T}}\ \cos\left[w_c t + d_j \pi \left\{h\left(\tfrac{t}{T}\right) - w\left(\tfrac{t}{T}\right)^2\right\}\right] \\ &\times \sqrt{\frac{2E_s}{T}}\ \cos\left[w_c t + d_i \pi \left\{h\left(\tfrac{t}{T}\right) - w\left(\tfrac{t}{T}\right)^2\right\}\right] dt \end{aligned} \tag{A.3}$$

Using the identity:

$$\cos\alpha\cos\beta = \frac{1}{2}\left[\cos\left(\alpha+\beta\right) + \cos\left(\alpha-\beta\right)\right] \tag{A.4}$$

and ignoring the high frequency term. (A.3) can be written as:

$$\rho(j,i) = \frac{1}{T}\int_0^T \cos\left[(d_j - d_i)\pi\left\{h\left(\frac{t}{T}\right) - w\left(\frac{t}{T}\right)^2\right\}\right] dt \tag{A.5}$$

if $(d_j - d_i) = 0 \quad \Rightarrow \rho = 1$

if $(d_j - d_i)$ $+ve$ or $(d_j - d_i)$ $-ve$

$$\rho(j,i) = \frac{1}{T}\int_0^T \cos\left[|(d_j - d_i)|\pi w\left(\frac{t}{T}\right)^2 - \pi|d_j - d_i|h\left(\frac{t}{T}\right)\right] dt \tag{A.6}$$

Let $a = \pi|d_j - d_i|w$, $b = \pi|d_j - d_i|$ and $x = \frac{t}{T}$ (A.6) can be written as:

$$\rho(j,i) = \frac{1}{T}\int_0^T \cos\left(ax^2 - bx\right) dt \tag{A.7}$$

and by completing the square, (A.7) can be written as:

$$\rho(j,i) = \frac{1}{T}\int_0^T \cos\left[\left(\sqrt{a}x - \frac{b}{2\sqrt{a}}\right)^2 - \left(\frac{b}{2\sqrt{a}}\right)^2\right] dt \tag{A.8}$$

applying the difference formula for the cosine $\cos(\alpha - \beta) = \cos\alpha\cos\beta + \sin\alpha sin\beta$, (A.8) can be expressed as:

$$\rho(j,i) = \frac{1}{T}\int_0^T \cos\left[\left(\frac{b}{2\sqrt{a}}\right)^2\right]\cos\left[\left(\sqrt{a}x - \frac{b}{2\sqrt{a}}\right)^2\right] +$$

$$\frac{1}{T}\int_0^T \sin\left[\left(\frac{b}{2\sqrt{a}}\right)^2\right]\sin\left[\left(\sqrt{a}x - \frac{b}{2\sqrt{a}}\right)^2\right] dt \tag{A.9}$$

By changing the variable $\sqrt{a}x - \frac{b}{2\sqrt{a}}$ in (A.9) into $\sqrt{\frac{\pi}{2}}u$ and acoordingly changing the limits, we get:

$$\rho(j,i) = \frac{\cos(\Omega)}{\sqrt{2\gamma w}}\left[\int_0^{u_h} \cos(\sqrt{\frac{\pi}{2}}u)^2 du - \int_0^{u_l} \cos(\sqrt{\frac{\pi}{2}}u)^2 du\right]$$
$$+\frac{\sin(\Omega)}{\sqrt{2\gamma w}}\left[\int_0^{u_h} \sin(\sqrt{\frac{\pi}{2}}u)^2 du - \int_0^{u_l} \sin(\sqrt{\frac{\pi}{2}}u)^2 du\right] \quad \text{(A.10)}$$

where $\Omega = \frac{\pi}{4}|d_j - d_i|\frac{(q+w)^2}{w}$ and $\gamma = |d_j - d_i|$. Solving the integral in (A.10) by applying Fresnel integral, the normalized cross correlation can be given as:

$$\rho(j,i) = \left[\frac{\cos(\Omega)}{\sqrt{2\gamma w}}(\mathbf{C}[u_h] - \mathbf{C}[u_l]) + \frac{\sin(\Omega)}{\sqrt{2\gamma w}}(\mathbf{S}[u_h] - \mathbf{S}[u_l])\right] \quad \text{(A.11)}$$

where the function $\mathbf{C}(.)$ and $\mathbf{S}(.)$ are the Fresnel cosine and sine integral which are given by:

$$\mathbf{C}(u) = \int_0^u \cos(\frac{\pi x^2}{2})dx$$

$$\mathbf{S}(u) = \int_0^u \sin(\frac{\pi x^2}{2})dx$$

Appendix B
Complex Correlation for M-ary Chirp Signals

In this appendix, we derive an expression for the complex cross correlation between signals $S_j(t)$ and $S_i^*(t)$. The complex correlation can be defined as:

$$\rho_c(j,i) = \frac{1}{2E_s}\int_0^{nT} S_j(t)S_i^*(t)dt \tag{B.1}$$

which is equal to:

$$\rho_c(j,i) = \frac{1}{2E_s}\int_0^{nT} \sqrt{\frac{2E_s}{T}}e^{j\left(w_c t + d_j\pi\left\{h\left(\frac{t}{T}\right) - w\left(\frac{t}{T}\right)^2\right\}\right)} \times \sqrt{\frac{2E_s}{T}}e^{-j\left(w_c t + d_i\pi\left\{h\left(\frac{t}{T}\right) - w\left(\frac{t}{T}\right)^2\right\}\right)} dt \tag{B.2}$$

(B.2) can be rewritten as:

$$\rho_c(j,i) = \frac{1}{T}\int_0^{T} e^{j\left(|d_i - d_j|\pi\left\{h\left(\frac{t}{T}\right) - w\left(\frac{t}{T}\right)^2\right\}\right)} \tag{B.3}$$

Applying Euler's formula to (B.3)

$$\rho_c(j,i) = \frac{1}{T}\int_0^{T} \left[cos(\Theta) + j\sin(\Theta)\right] dt \tag{B.4}$$

where $\Theta = |d_i - d_j|\pi \left\{ h\left(\frac{t}{T}\right) - w\left(\frac{t}{T}\right)^2 \right\}$ The integral for the cosine and sine in (B.4) can be solved following the same procedure in Appendix A. The correlation is given by:

$$\rho(j,i) = \left[\frac{\cos(\Omega)}{\sqrt{2\gamma w}}\left(\mathbf{C}[u_h] - \mathbf{C}[u_l]\right) + \frac{\sin(\Omega)}{\sqrt{2\gamma w}}\left(\mathbf{S}[u_h] - \mathbf{S}[u_l]\right)\right]$$

$$+ \left[\frac{\cos(\Omega)}{\sqrt{2\gamma w}}\left(\mathbf{S}[u_h] - \mathbf{S}[u_l]\right) + \frac{\sin(\Omega)}{\sqrt{2\gamma w}}\left(\mathbf{S}[u_h] - \mathbf{S}[u_l]\right)\right] \tag{B.5}$$

where $\Omega = \frac{\pi}{4}|d_j - d_i|\frac{(q+w)^2}{w}$, $\gamma = |d_j - d_i|$ and the function $\mathbf{C}(.)$ and $\mathbf{S}(.)$ are the Fresnel cosine and sine integral which are given by:

$$\mathbf{C}(u) = \int_0^u \cos(\frac{\pi x^2}{2})dx$$

$$\mathbf{S}(u) = \int_0^u \sin(\frac{\pi x^2}{2})dx$$